

Changing sources and processes sustaining surface CO₂ and CH₄ fluxes along a tropical river to reservoir system

Cynthia Soued¹, Yves T. Prairie¹

¹Groupe de Recherche Interuniversitaire en Limnologie et en Environnement Aquatique (GRIL), Département des Sciences
5 Biologiques, Université du Québec à Montréal, Montréal, H2X 3X8, Canada.

Correspondence to: Cynthia Soued (cynthia.soued@gmail.com)

Abstract. Freshwaters are important emitters of carbon dioxide (CO₂) and methane (CH₄), two potent greenhouse gases (GHG). While aquatic surface GHG fluxes have been extensively measured, there is much less information about their underlying sources. In lakes and reservoirs, surface GHG can originate from horizontal riverine flow, the hypolimnion, littoral
10 sediments, and water column metabolism. These sources are generally studied separately, leading to a fragmented assessment of their relative role in sustaining CO₂ and CH₄ surface fluxes. In this study, we quantified sources / sinks of CO₂ and CH₄ in the epilimnion along a hydrological continuum in a permanently stratified tropical reservoir (Borneo Island). Results showed that horizontal inputs are an important source of both CO₂ and CH₄ (> 90 % of surface emissions) in the upstream reservoir branches. However, this contribution fades along the hydrological continuum, becoming negligible in the main basin of the
15 reservoir, where CO₂ and CH₄ are uncoupled and driven by different processes. In the main basin, vertical CO₂ inputs and sediment CH₄ inputs contributed to on average 60 and 23 % respectively to the surface fluxes of the corresponding gas. Water column metabolism exhibited wide amplitude and range for both gases, making it a highly variable component, but with a large potential to influence surface GHG budgets in either direction. Overall our results show that sources sustaining surface CO₂ and CH₄ fluxes vary spatially and between the two gases, with internal metabolism acting as a fluctuating but key
20 modulator. However, this study also highlights challenges and knowledge gaps related to estimating ecosystem-scale CO₂ and CH₄ metabolism, which hinder aquatic GHG flux predictions.

1 Introduction

Surface inland waters are globally significant sources of greenhouse gases (GHG) to the atmosphere, namely carbon dioxide
25 (CO₂) and methane (CH₄) (Bastviken et al., 2011; DelSontro et al., 2018a; Raymond et al., 2013). Freshwaters act as both transport vessels for terrestrial carbon (C) and as active biogeochemical processors, making them key sites of GHG exchange with the atmosphere (Tranvik et al., 2018). The impoundment of rivers for hydropower generation, irrigation, flood control or other purposes, changes the landscape and its C cycling (Maavara et al., 2017), often resulting in increased aquatic CO₂ and CH₄ emissions due to the decay of flooded organic matter (Prairie et al., 2018; Venkiteswaran et al., 2013). Globally, reservoirs

30 are estimated to emit between 0.5 and 2.3 PgCO₂eq yr⁻¹ (Barros et al., 2011; Bastviken et al., 2011; Deemer et al., 2016; St. Louis et al., 2000), and this number is predicted to increase with a rapid growth of the hydroelectric sector in the upcoming decades (Zarfl et al., 2015). Several studies have focused on quantifying GHG surface diffusion from reservoirs around the world and have found extremely high variability temporally and spatially (Barros et al., 2011; Deemer et al., 2016), as is found in natural lakes (DelSontro et al., 2018a; Raymond et al., 2013). However, less research exists on the relative contribution of
35 the different sources and processes sustaining surface diffusive fluxes and their variability in reservoirs.

GHG sources to surface waters can be both internal and external. The magnitude of allochthonous inputs, namely terrestrial organic and inorganic C, is known to increase with soil-water connectivity (Hotchkiss et al., 2015), and with soil C content and leaching capacity (Kindler et al., 2011; Li et al., 2017; Monteith et al., 2007). Soil-derived gas inputs are also temporally variable, generally increasing with discharge, like during storm events (Vachon and del Giorgio, 2014) or rainy seasons (Kim
40 et al., 2000; Zhang et al., 2019). Terrestrial inputs in the form of organic C can indirectly sustain surface GHG emissions by fueling lake / reservoir *in situ* organic matter respiration (Karlsson et al., 2007; Pace and Prairie, 2005; Rasilo et al., 2017).

The net internal balance between production and consumption processes of CO₂ and CH₄ ultimately determines their surface fluxes. For CO₂, aerobic ecosystem respiration (ER) and gross primary production (GPP) are highly variable in space and time, and generally a function of temperature, organic C content and nutrients (Hanson et al., 2003; Pace and Prairie, 2005; Prairie
45 et al., 1989; Solomon et al., 2013). Net heterotrophy (ER > GPP) is mainly associated with systems receiving high external inputs of organic C (Bogard et al., 2020; Tank et al., 2010; Wilkinson et al., 2016), while net autotrophy (ER < GPP) has been associated with highly productive nutrient-rich systems (Hanson et al., 2003; Sand-Jensen and Staehr, 2009). However, a large part of the variability in measured metabolic rates remains unexplained (Bogard et al., 2020; Coloso et al., 2011; Solomon et al., 2013) impeding our ability to accurately predict their net balance. Additionally, anaerobic C transformation adds another
50 level of complexity to the C metabolic balance by decoupling GPP and ER (Bogard and del Giorgio, 2016; Martinsen et al., 2020; Vachon et al., 2020). For instance, acetoclastic methanogenesis can transform organic C to CH₄ instead of CO₂, and hydrogenotrophic methanogenesis converts CO₂ to CH₄ without producing O₂.

For CH₄, production occurs in both profundal and littoral sediments, and reach the water surface by vertical or lateral diffusive processes (Bastviken et al., 2008; DelSontro et al., 2018b; Encinas Fernández et al., 2014; Guérin et al., 2016). However, there
55 is increasing evidence that CH₄ production in the oxic water column can also contribute significantly to lake CH₄ emissions (Bižić et al., 2019; Bogard et al., 2014; DelSontro et al., 2018b; Donis et al., 2017; Tang et al., 2014). Methanogenesis can be counter-balanced by the oxidation of CH₄ to CO₂ mainly in oxic and hypoxic environments (Conrad, 2009; Reis et al., 2020; Thottathil et al., 2019). While several studies have measured rates of CH₄ production and oxidation in lakes and reservoirs, few have quantified the net balance of these two processes at an ecosystem-scale (Bastviken et al., 2008; Schmid et al., 2007),
60 a balance tightly linked to physical processes within the water column (Vachon et al., 2019).

For both gases, physical mixing in lakes and reservoirs indirectly impacts C metabolic processes by shaping the O₂ profile, and directly affects GHG surface diffusion by controlling the transport of CO₂ and CH₄ from deep to surface water layers (Barrette and Laprise, 2005; Kreling et al., 2014; Pu et al., 2020). Despite its potential importance (Kankaala et al., 2013), very

few studies quantified vertical gas transport and the role of this process in fueling surface GHG emissions. The movement of
65 gases within a system depends on the structure of the water column, which changes spatially along the aquatic continuum.
Reservoirs in particular exhibit strong gradients in morphometry and hydrology, translating into high spatial heterogeneity in
surface GHG fluxes to the atmosphere (Paranaíba et al., 2018; Teodoru et al., 2011).

Understanding what regulates surface CO₂ and CH₄ concentrations and fluxes to the atmosphere thus requires knowledge of
the interplay between all physical and biogeochemical processes involved, and how they vary spatially. While a number of
70 studies have assessed some processes individually or by difference, very few have measured all relevant components of the
epilimnetic mass-balance simultaneously. Here we report on a field study in a tropical East Asian hydropower reservoir
quantifying external inputs, sediments inputs, net CO₂ and CH₄ metabolism, vertical diffusion from deeper layers and gas
exchange at the air-water interface. This allowed us to estimate the relative contribution of each process in shaping surface
GHG emissions from the reservoir, and to test whether the epilimnetic mass balance can be closed. The two major rivers
75 feeding the reservoir flow into two elongated branches, acting as a transition zones, before reaching the main basin. This
configuration, common in reservoirs, allowed us to quantify and compare epilimnetic CO₂ and CH₄ regulation in two
morphometrically different areas (reservoir branches and main basin). Overall, the aim of this study is to provide an ecosystem-
scale portrait of the processes sustaining surface CO₂ and CH₄ emissions and examine how they change when transitioning
from a river delta to an open basin.

80 **2 Materials and methods**

2.1 Site and sampling description

The study was conducted in Batang Ai hydroelectric reservoir in Sarawak Malaysia (latitude 1.16° and longitude 111.9°). The
reservoir is located on the Borneo Island in a tropical equatorial climate with a constantly high temperature averaging 23 °C
and 32 °C during nighttime and daytime respectively (Sarawak Government, 2019). The region experiences two weak monsoon
85 seasons (November to February and June to October) with a yearly average rainfall of 3300 to 4600 mm (Sarawak Government,
2019). The reservoir was impounded in 1985 with a dam wall of 85 m, a surface area of ~68.4 km² and a watershed area of
1149 km² of mostly undisturbed forested land (limited rural habitations and small scale croplands).

We distinguish between three sections of the study site: inflows, reservoir branches, and reservoir main basin shown in Fig. 1.
The inflows are the two main reservoir inlets: Batang Ai and Engkari rivers (3 to 10 m deep where sampled). The two rivers
90 flow into two arms that we refer to as the reservoir branches (10.8 km², mean and max depths of 18 and 52 m respectively).
The reservoir branches merge into the main basin of the reservoir (58.9 km², mean and max depths of 30 and 73 m respectively).
Surface sampling was performed in 36 sites across the three study sections, and water column profile sampling (from 0 up to
32 m, each 0.5 to 3 m) was done at 9 sites in the reservoir branches and main basin (Fig. 1). Sampling was repeated (with a
few exceptions) during four campaigns: 1) November 14th to December 5th 2016 (Nov-Dec 2016), 2) April 19th to May 3th
95 2017 (Apr-May 2017), 3) February 28th to March 13th 2018 (Feb-Mar 2018), and 4) August 12th to 29th 2018 (Aug 2018).

2.2 Physical and chemical analyses

Water temperature, dissolved oxygen, and pH were measured using a multi-parameter probe (YSI model 600XLM-M) equipped with a depth gauge and attached to a 12 Volt submersible pump (Proactive Environmental Products model Tornado) for water samples collection. Concentrations of dissolved organic carbon (DOC), total phosphorus (TP), total nitrogen (TN), and chlorophyll a (Chla) were measured during all campaigns in all surface sampling sites (Fig. 1). Methods for these analyses are described in detail in Soued and Prairie (2020). Briefly, TP and Chla (extracted with hot ethanol) were analyzed via spectrophotometry, and TN and DOC (filtered at 0.45 μm) were measured on an Alpkem Flow Solution IV autoanalyser and on a Total Organic Carbon analyser 1010-OI respectively.

For each site, we defined the depths of the thermocline and the top and bottom of the metalimnion based on measured temperature profiles using the R package rLakeAnalyzer (Winslow et al., 2018). The epilimnion was defined from the surface to the top of the metalimnion, and was assumed to be a mixed layer.

2.3 Gas concentration, isotopic signature, and water-air fluxes

CO_2 and CH_4 gas concentrations and isotopic signatures ($\delta^{13}\text{C}$) were measured in duplicates at the surface in 36 sites and along vertical profiles in 9 sites (P1 to P9, Fig. 1) using the headspace technique described in details in Soued and Prairie (2020). In brief, sampling was done by equilibrating the water sample for two minutes with an air headspace inside a 60 mL syringe. The gas phase was then injected in a 12 mL pre-vacuumed air-tight vial, and analyzed on a gas chromatograph (Shimadzu GC-8A with a flame ionization detector) for gas concentrations, and on a Cavity Ring Down Spectrometer (CRDS) equipped with a Small Sample Isotopic Module (SSIM, Picarro G2201 -i) for $\delta^{13}\text{CO}_2$ and $\delta^{13}\text{CH}_4$.

Surface gas flux data used in this study are described in more details in Soued and Prairie (2020), a previous study on the footprint of Batang Ai reservoir. Surface diffusive fluxes of CO_2 and CH_4 were measured at all surface sampling sites during each campaigns. Flux rates were derived from linear changes in CO_2 and CH_4 concentrations in a static floating chamber (design described in Soued and Prairie (2020) and IHA (2010)) connected in a closed loop to a portable gas analyzer (model UGGA, from Los Gatos Research). Measured gas concentrations, isotopic signature, and fluxes were spatially interpolated to the whole reservoir area by inverse distance weighting (given the absence of a suitable variogram for kriging) using package gstat version 1.1-6 in the R version 3.4.1 software (Pebesma, 2004). Mean values were calculated for each campaign based on the interpolated maps (Soued and Prairie, 2020).

2.4 Horizontal GHG inputs

In order to estimate the external horizontal inputs of CO_2 and CH_4 , we considered that the total volume of water inflow and outflow (discharge measured at the dam) were equal, and equivalent to the mean of measured daily discharge (Q , in $\text{m}^3 \text{d}^{-1}$) during each campaign (considering minimal changes in inflow / outflow rates during a campaign). The approach of using discharge as a measure of total water inflow has the advantage of integrating all external flow (rivers, lateral soils, and

groundwater) as water inputs to the reservoir. However, the fraction of inflow feeding the reservoir surface versus bottom layer, and its average gas concentration can only be approximated based on measurements from the two main river inlets (Fig. 1) due to the lack of data on other lateral inflows. Given that part of the inflowing water is colder and denser than the reservoir surface layer, only a fraction of it enters the epilimnion of the reservoir branches, and the rest plunges into the hypolimnion. We estimated that fraction (f_{epi}) based on temperature profiles in the East river delta and branch (sites P1 and P2, Fig. 1), and assumed it is representative of other water inflows to the reservoir. The areal rate of horizontal CO₂ and CH₄ inputs (H , in mmol m⁻² d⁻¹) over each section of the reservoir were then calculated following Eq. (1):

$$H = \frac{C_{in} Q f_{epi}}{A} \quad (1)$$

with A (in m²) the surface area of the reservoir section considered, and C_{in} (in mmol m⁻³) the concentration of gas in the inflowing water. To estimate gas inputs from the inflows to the branches, C_{in} was considered as the average of gas concentrations measured at the two upstream extremities of the branches (Fig. 1). To estimate gas inputs from the branches to the main basin, C_{in} was considered as the gas concentrations measured at the confluence between the two branches (right upstream of the main basin).

140 2.5 Vertical GHG fluxes

We estimated CO₂ and CH₄ fluxes from the metalimnion to the epilimnion (V) based on the vertical gas diffusivity (K_z) and the gradient in gas concentration across the epilimnion-metalimnion interface using Eq. (2) (Wüest and Lorke, 2009):

$$V = K_z (C_{meta} - C_{epi}) \quad (2)$$

where C_{meta} and C_{epi} are the gas concentrations at the top of the metalimnion and at the bottom of the epilimnion respectively, measured in profile sites (P1 to P9, Fig. 1). K_z was derived from the following Eq. (3) (Osborn, 1980):

$$K_z = \Gamma \frac{\epsilon}{N^2} \quad (3)$$

where Γ is the mixing ratio set to 0.2 (Oakey, 1982), ϵ is the dissipation rate of turbulent kinetic energy, and N^2 is the buoyancy frequency. N^2 was calculated from measured temperature profiles (YSI probe) using function `buoyancy.freq` from the `rLakeAnalyzer` package (Winslow et al., 2018) in the R software (R Core Team, 2017). ϵ was derived from measured vertical shear microstructure profiles performed in the Aug 2018 campaign in all profile sites shown in Fig. 1 (except P1 due to floating logs). Shear profiles were measured with a high frequency (512 Hz) MicroCTD profiler (Rockland Scientific) equipped with two velocity shear probes, two thermistors, tilt and vibration sensors, and a pressure sensor. At each site, the profiler was cast 10 times, 5 with an uprising configuration (from bottom to top of the water column) and 5 with a downward configuration (top to bottom), with a 4 min waiting time between profiles to allow water column disturbance to subside. Data quality check and ϵ calculation for each profile cast were performed with ODAS v4.3.03 Matlab library (developed by Rockland Scientific) based on Nasmyth shear spectrum (Oakey, 1982), with ϵ values averaged among the two shear probes and binned over 1-2 m segments along the profile. For each site, continuous ϵ profiles were interpolated by fitting a smooth spline through all ϵ values from replicate casts as a function of depth.

At the epilimnion-metalimnion interface (top of the metalimnion ± 2 m), calculated ϵ averaged 7.7×10^{-9} (range from 3.4×10^{-9} to 1.6×10^{-8}) $\text{m}^2 \text{s}^{-3}$ across all sites sampled with the microCTD, with no significant difference between the main basin and branches sites. In order to estimate vertical gas diffusion, we applied the latter ϵ average to Eq. (2) and (3) for all measured gas profiles (except P1). The resulting V values for each gas were averaged across sites in the main basin and branches separately to derive estimates of V for each of these two reservoir sections.

2.6 Sediment GHG inputs

We calculated CO_2 and CH_4 inputs from the sediments to epilimnetic waters using gas profiles in sediment cores collected in Apr-May 2017 and Feb-Mar 2018 at 7 sites (P1 to P3 in the reservoir branches and P4, P5, P7, and P9 in the main basin, Fig. 1). Sediment cores were collected using a Glew gravity corer attached to a 6-cm-wide plastic liner. The liner was pre-drilled with 1 cm holes covered with electric tape at each centimeter up to 40 cm. Upon recovery of the sediment core, 3 mL tip-less syringes were inserted into each hole to extract sediments from each centimeter. The sediment content of each syringe was emptied into a 25 mL glass vial prefilled with 6 mL nano-pure water and immediately air-tight sealed by a butyl rubber stopper crimped with an aluminum cap. Glass vials were pressurized with 40 mL of ambient air using a plastic syringe equipped with a needle to pierce the rubber cap. Glass vials were shaken for 2 min for equilibration before extracting the gas with a syringe and injecting it into a pre-evacuated air-tight vial for analysis of CO_2 and CH_4 concentrations and isotopic signatures as described above. Additionally, samples of the water overlaying the sediments (~ 1 cm above) were collected for similar analyses of CO_2 and CH_4 .

Sediment CO_2 and CH_4 flux rates to the overlaying water column were derived from the vertical gradient of gas concentration measured in the sediment cores and overlaying water. The slope of CO_2 or CH_4 concentration as a function of depth (g , in $\mu\text{mol L}^{-1} \text{m}^{-1}$) was calculated for measured values in the first 5 cm of sediments and overlaying water. Most cores exhibited clear linear slopes (p -value < 0.05 and $R^2_{\text{adj}} > 0.5$). In the few cases where a linear slope was not evident, g was replaced by the gradient between the mean gas concentration in the first 3 cm of sediments and the overlaying water. The sediment gas flux rate (S_f in $\text{mmol m}^{-2} \text{d}^{-1}$) were calculated with Eq. (4):

$$S_f = \frac{g \times d}{p} \quad (4)$$

With d the diffusion coefficient set to $1.5 \times 10^{-5} \text{ cm}^2 \text{ s}^{-1}$ (Donis et al., 2017), and p the sediment porosity assumed to be 2 % based on previous results in Batang Ai (Tan, 2015).

At an ecosystem scale, sediment CO_2 and CH_4 inputs to the water column (S) were estimated based on average and standard deviation values of sites located in each section of the reservoir (branches and main basin). For each section, mean sediment CO_2 and CH_4 flux rates were multiplied by the areal ratio of epilimnetic sediments (A_{epi}) versus total water area (A_0). The latter ratio was calculated based on the hypsometric model (Ferland et al., 2014; Imboden, 1973) as shown in Eq. (5) to (7):

$$q = \left(\frac{z_{\text{max}}}{z_{\text{mean}}} \right) - 1 \quad (5)$$

$$190 \quad A_{epi} = A_0 \left(1 - \left(1 - \left(\frac{z_{epi}}{z_{max}} \right) \right)^q \right) \quad (6)$$

$$S = \frac{A_{epi}}{A_0} S_f \quad (7)$$

with q a parameter describing the general bathymetric shape of the reservoir section, z_{max} and z_{mean} the maximum and mean depths respectively, and z_{epi} the mean depth of the epilimnion (8.0 and 10.5 m in the branches and main basin respectively).

Littoral sediments are known to be a source of CH_4 not only through diffusion but also via ebullition. While this emission pathway was found to be important in other reservoirs (Deemer et al., 2016), it is surprisingly low in Batang Ai, equaling less than 2 % of CH_4 surface diffusive emissions, and only 0.1 % of the reservoir total GHG footprint (Soued and Prairie, 2020). Therefore, sediment ebullition was considered negligible in the epilimnetic CH_4 budget of Batang Ai.

2.7 Metabolic rates

Net metabolic rates of CO_2 and CH_4 production in the epilimnetic water column were estimated with *in situ* incubations. Incubations were performed in 5 sites (P2 and P3 in the branches and P4, P5 and P7 in the main basin, Fig. 1). Water from 3 m deep was pumped into 5 L transparent glass jars with an air tight clamp lid. Before closing, jars were filled from the bottom and allowed to overflow, then sampled for initial CO_2 and CH_4 concentrations. Closed jars were fixed at 3 m to an anchored line at the sampling site, and incubated in *in situ* temperature and light conditions for 22.0 to 24.2 hours. Upon retrieval, samples of final CO_2 and CH_4 concentrations were collected from the jars. Volumetric daily rates of net CO_2 and CH_4 production were calculated based on the difference between final and initial gas concentrations rescaled to a 24 h period.

In addition to incubations, open water high frequency O_2 measurements were carried out to derive CO_2 metabolism on larger spatial and temporal scales. Rates of GPP, ER, and net ecosystem production (NEP) were estimated in the reservoir surface layer by monitoring and inverse modeling diel O_2 changes in the epilimnion. O_2 was measured at a one minute interval using high frequency O_2 and temperature sensors (model miniDOT from Precision Measurement Engineering), along with light sensors (model HOBO Pendant from Onset). Sensors were deployed in profile sites P1 to P3 in the branches and P4, P5, P7, and P9 in the main basin (Fig. 1). Note that not all sites were sampled in all sampling campaigns. Sensors were attached to an anchored line at a depth between 0.7 and 3 m and deployment time varied between 4 days and two weeks. Upon retrieval of the sensors, a first data quality check and selection was made based on the sensor internal quality index and visual screening. Rates of ecosystem metabolism were then estimated based on an open system diel O_2 model (Odum, 1956), where change in O_2 concentration is a function of GPP, ER, and air-water gas exchange (K_{O_2}) following Eq. (8) (Hall and Hotchkiss, 2017):

$$215 \quad \frac{dO_2}{dt} = \frac{GPP}{z_{epi}} + \frac{ER}{z_{epi}} + K_{O_2} (O_{2sat} - O_2) \quad (8)$$

with O_{2sat} the theoretical O_2 concentration at saturation considering the *in situ* temperature and atmospheric pressure, and O_2 is the actual measured O_2 concentration in the water. A detailed description of the model equations can be found in (Hall and Hotchkiss, 2017). Daily estimates of GPP, ER, and K_{600} (based on K_{O_2}) were derived by maximum likelihood fitting of the data to the model in Eq. (8) using the R package StreamMetabolizer (Appling et al., 2018). Note that even though the package

used was originally developed for streams, it is easily transferable to lakes given that the model used (Eq. (8)) is generalized for all water bodies, with the parameter z_{epi} describing the depth of a mixed water column of either a lentic or lotic system, and with the K_{600} estimate relying only on data fitting to the model and not on system type. In some cases, where the best predicted K_{600} was negative, the fitting process was rerun with a user defined positive K_{600} , either equal to a value estimated for the previous or subsequent day at the same site (range of 0.03 – 0.96 d^{-1}) or fixed to 0.1 d^{-1} (if no other available estimate). When
225 considering the epilimnion depth, predicted values of K_{600} translate into a 1st to 3rd quantiles range of 1.17 to 5.55 $m d^{-1}$, which is similar to the range of K_{600} values back-calculated from surface gas flux measurements with the floating chamber technique. A final selection of daily metabolic estimates was done based on the model goodness of fit assessed by calculating Pearson correlation coefficient between modeled and measured O_2 values and discarding days with a correlation lower than 0.9. Based
230 on GPP and ER estimates, we calculated daily NEP as the balance between these two processes, and converted it to net CO_2 production rate by assuming an $O_2:CO_2$ metabolic quotient of 1.

Areal metabolic rates were derived by integrating volumetric rates over the depth of the epilimnion. Average estimates of areal metabolic rates per campaign were obtained for the branches and main basin by first averaging data within each site and then across sites for each reservoir section. Note that one value derived from incubations was excluded from the calculation of the
235 average net CH_4 production rate in the branches due to its high value of initial CH_4 concentration (an order of magnitude higher than in all other incubations and all epilimnetic data from this site). The high CH_4 concentration, unrepresentative of real conditions, was probably caused by CH_4 contamination during sampling, and triggered a high oxidation rate that would overestimate the real ecosystem average rate if included.

2.8 Epilimnetic GHG budgets

240 Areal rates of horizontal, vertical, sediment, and metabolic inputs were combined into a sum of sources / sinks and compared to the rate of surface gas flux for each gas in each reservoir section. A mean and standard error were calculated for every component of the budgets based on measurements averaged across sites and / or sampling campaigns in order to obtain ecosystem-scale estimates of the components means and uncertainties. In the case of CO_2 metabolism, the ecosystem-scale average was calculated as the mean of the two average values derived from the incubation and diel O_2 monitoring methods.
245 For every component, density curves were derived considering a normal distribution based on the mean and its standard error in order to visualize the relative magnitude and uncertainty of each ecosystem-scale areal rate (Fig. 3).

3 Results

3.1 Physical and chemical properties

Surface water temperature exhibited a marked increase from the inflows to the branches, averaging 27.1 and 30.7 °C, respectively (Table 1). There was no difference in surface water temperature between the branches and the main basin. The
250 depth of the epilimnion tended to increase and become more stable along the water flow, going from 1.3 (\pm 1.6) m in Batang

255 Ai river delta, to 8.0 (\pm 2.3) m in its branch, and 10.6 (\pm 1.7) m in the main basin (Table 1). Light penetration exhibited the same spatial pattern, with an increasing Secchi depth along the water flow averaging 1.3, 5.1, and 5.5 m in the inflows, branches, and main basin respectively (Table 1). All sections of the study system exhibited oligotrophic water properties (Table 1).

3.2 Surface GHG concentrations, fluxes, and isotopic signatures

Surface CO₂ and CH₄ patterns are summarized in Fig. 2, presenting campaign averages of spatially interpolated gas concentration, flux, and isotopic signature along the different reservoir sections. Despite the temporal variability, the gas patterns along the water flow are robust, remaining similar throughout time (Fig. 2).

260 Average CO₂ air-water flux and surface concentration were systematically higher in the inflows (mean [range]: 135.3 [18.9 – 368.8] mmol m⁻² d⁻¹ and 58.0 [24.5 – 113.0] μ mol L⁻¹, respectively) compared to the branches (4.7 [-3.4 – 15.2] mmol m⁻² d⁻¹ and 15.4 [12.2 – 19.3] μ mol L⁻¹) and main basin (7.5 [0.3 – 15.1] mmol m⁻² d⁻¹ and 16.0 [14.2 – 17.7] μ mol L⁻¹) (Fig. 2a, b). Surface CO₂ concentration in the reservoir (branches and main basin) was most strongly correlated inversely with water temperature ($R^2_{\text{adj}} = 0.22$, p-value < 0.001, Fig. S1a and Table S1). Except for the Apr-Mar 2017 campaign, there was a modest
265 increase (2.2 to 3.3 ‰) of surface $\delta^{13}\text{CO}_2$ towards more enriched values from the inflows to the branches (Fig. 2c).

Similarly, surface CH₄ flux and concentration continually decreased along the water channel, being an order of magnitude higher in the inflows compared to the branches, and about twice as high in the branches compared to the main basin (Fig. 2d, e). Of all measured water properties, TN was the most strongly linked to reservoir surface CH₄ concentration ($R^2_{\text{adj}} = 0.14$, p-value < 0.001, Fig. S1b and Table S1). In the main basin, surface CH₄ concentration significantly decreased with distance to
270 shore in Nov-Dec 2016 ($R^2_{\text{adj}} = 0.54$, p-value < 0.001), but this correlation was weaker ($R^2_{\text{adj}} \leq 0.13$, p-value ≥ 0.03) during other sampling campaigns (Fig. 6a). Surface $\delta^{13}\text{CH}_4$ values varied widely, between -83.3 and -47.6 ‰, but did not show a consistent spatial pattern (Fig. 2f) apart from a positive correlation with distance to shore in the main basin in Nov-Dec 2016 ($R^2_{\text{adj}} = 0.29$, p-value = 0.01, Fig. 6b).

The degree of coupling between CO₂ and CH₄ followed a clear spatial pattern. While CO₂ and CH₄ surface concentrations
275 were strongly linked in the inflows ($R^2_{\text{adj}} = 0.54$, p-value = 0.006), they became only weakly correlated in the branches ($R^2_{\text{adj}} = 0.17$, p=0.005) and not correlated at all in the main basin ($R^2_{\text{adj}} = 0.01$, p-value = 0.11) (Fig. S2).

3.3 Horizontal GHG flow

Horizontal inputs from the inflows to the surface layer of the branches were estimated to vary between 0.34 – 0.71 mol s⁻¹ for CO₂ and 0.02 – 0.25 mol s⁻¹ for CH₄. When expressed as areal rates over the branches (to facilitate comparison with other
280 components), horizontal inputs amounted to 2.7 – 5.7 and 0.16 – 1.97 mmol m⁻² d⁻¹ for CO₂ and CH₄, respectively (Table S2 and S3). These values are in the same order of magnitude as surface fluxes calculated in the branches (Fig. 3a, c, Table S2 and S3). However, the effect of horizontal inputs faded spatially, with much lower inputs from the branches to the main reservoir basin, averaging 0.31 and 0.004 mmol m⁻² d⁻¹ for CO₂ and CH₄, respectively (Fig. 3b, d and Table S2 and S3). For CH₄, this

fits spatial and temporal surface flux measurements, being systematically higher in the branches, and maximal during the two
285 sampling campaigns with the highest recorded horizontal inputs from the inflows (Table S3). In contrast, CO₂ surface flux was
typically lower (sometimes negative) in the branches compared to the main basin, despite substantial riverine inputs to the
branches (Table S2).

3.4 Vertical GHG inputs

Vertical fluxes depend on the gas diffusivity and concentration gradient. Gas diffusivity is a function of the strength of
290 stratification (N^2) and energy dissipation rate (ϵ). Measured values of N^2 and ϵ varied widely, from 5.9×10^{-5} to $2.3 \times 10^{-3} \text{ s}^{-2}$
and from 3.4×10^{-9} to $1.6 \times 10^{-8} \text{ m}^2 \text{ s}^{-3}$ respectively, but with no clear differences between the reservoir branches and main
basin (Fig. S3a, b). Similarly, CO₂ and CH₄ concentration gradients varied substantially in both space and time (from -18.4 to
94.3 $\mu\text{mol L}^{-1} \text{ m}^{-1}$ for CO₂ and -0.19 to 0.4 $\mu\text{mol L}^{-1} \text{ m}^{-1}$ for CH₄). CO₂ concentration generally increased from the epilimnion
to the metalimnion as a result of the respiratory CO₂ buildup in the deep layer. On rare occasions, an inverse gradient was
295 observed, possibly due to autotrophic activity in the metalimnion. For CH₄, metalimnion to epilimnion concentration gradients
were generally modest averaging 0.04 $\mu\text{mol L}^{-1} \text{ m}^{-1}$, and even negative in one third of the profiles leading to the diffusion of
epilimnetic CH₄ toward deeper layers instead of the reverse. The low to negative CH₄ vertical flux results from a highly active
methanotrophic layer reducing CH₄ concentration in the metalimnion, as evidenced by the strong enrichment effect observed
in $\delta^{13}\text{C}_{\text{CH}_4}$ profiles (Fig. S4). The combination of vertical diffusivity and gas concentration gradients resulted in vertical fluxes
300 averaging 3.4 (-1.8 to 20.5) $\text{mmol m}^{-2} \text{ d}^{-1}$ for CO₂, and 0.01 (-0.01 to 0.09) $\text{mmol m}^{-2} \text{ d}^{-1}$ for CH₄, with no significant differences
between the reservoir branches and main basin (Fig. S3).

3.5 GHG inputs from littoral sediments

Areal sediment gas fluxes ranged from 1.2 to 4.0 and -0.29 to 1.10 $\text{mmol m}^{-2} \text{ d}^{-1}$ for CO₂ and CH₄, respectively (Fig. S5), in
the range of previously reported values in lakes and reservoirs (Adams, 2005; Algesten et al., 2005; Gruca-Rokosz and
305 Tomaszek, 2015; Huttunen et al., 2006). Sediment fluxes were not different in the branches versus the main basin for both
CO₂ (mean of 2.2 vs 2.4 $\text{mmol m}^{-2} \text{ d}^{-1}$) and CH₄ (mean of 0.17 vs 0.48 $\text{mmol m}^{-2} \text{ d}^{-1}$) (Fig. S5). Applying measured averages
to the area of epilimnetic sediments in each section yields estimates of sediment inputs to the epilimnion of 0.6 (\pm 0.03) and
0.5 (\pm 0.11) $\text{mmol m}^{-2} \text{ d}^{-1}$ for CO₂, and 0.04 (\pm 0.02) and 0.10 (\pm 0.06) $\text{mmol m}^{-2} \text{ d}^{-1}$ for CH₄ in the branches and main basin
respectively (Fig. 3 and Table S2 and S3). These inputs from littoral sediments likely represent an upper limit since they are
310 based on deep pelagic sediment cores (littoral area were too compact for coring), where a higher organic matter accumulation
and degradation is expected (Blais and Kalff, 1995; Soued and Prairie, 2020). Even as upper estimates, the calculated rates of
sediment GHG inputs remain a relatively modest fraction of the average emissions to the atmosphere for the branches and
main basin both for CO₂ (13 % and 7 %, respectively) and CH₄ (4 % and 23 %, respectively) (Tables S2 and S3).

3.6 Metabolism

315 3.6.1 CO₂ metabolism

Estimated GPP and ER rates based on diel O₂ monitoring ranged from 3.6 to 34.5 μmol L⁻¹ d⁻¹ and from 5.8 to 29.5 μmol L⁻¹ d⁻¹ respectively (Fig. 4a), which is well within the range of reported rates for oligotrophic systems (Bogard and del Giorgio, 2016; Hanson et al., 2003; Solomon et al., 2013). As expected, GPP and ER rates were correlated ($R^2_{\text{adj}} = 0.23$, p-value < 0.001, Fig. 4a), with photosynthesis stimulating the respiration of produced organic matter. In most cases, GPP exceeded ER, especially in the branches and near aquacultures (Fig. 4a), where higher nutrients (TP and TN) and Chla concentrations were measured (Table 1). Daily metabolic rates showed no correlation with mean daily rain or light (Kendall rank correlation p-value > 0.1).

In the reservoir branches, results from the diel O₂ monitoring method suggested systematic net CO₂ uptake ranging from -19.2 to -1.4 μmol L⁻¹ d⁻¹, whereas results from two incubations were slightly above that range (-0.5 to 3.3 μmol L⁻¹ d⁻¹) (Fig. 4b). In the main basin, incubation results ranged from -8.8 to 7.2 μmol L⁻¹ d⁻¹, while the diel O₂ technique captured a wider variability in net CO₂ metabolic rates from -19.2 to 6.1 μmol L⁻¹ d⁻¹, with an estimated CO₂ uptake in 39 out of 54 cases (Fig. 4b). Areal net CO₂ metabolic rates, as the average of the two methods, yielded an ecosystem-scale estimate of -23.2 and -11.8 mmol m⁻² d⁻¹ in the reservoir branches and main basin, respectively (Table S2).

To complement the metabolic rate data, surface O₂ and CO₂ departure from saturation were examined in both reservoir sections. O₂ oversaturation was observed in 44 % of cases in the main basin and 81 % in the branches (Fig. 5), which corresponds with the spatial patterns of net metabolic rates (Fig. 4b). CO₂ oversaturation was also widespread (74 % of cases), making many sampled sites oversaturated in both O₂ and CO₂ (55 % in the branches and 32 % in the main basin, Fig. 5).

3.6.2 CH₄ metabolism

Net metabolic CH₄ rates (from incubations) ranged from -0.026 to 0.078 μmol L⁻¹ d⁻¹, indicating that the CH₄ balance in the epilimnion of Batang Ai varied from net oxidation to net production (Table S3). CH₄ metabolic rates measured in Batang Ai are within the range of values observed in other systems for oxidation (Guérin and Abril, 2007; Thottathil et al., 2019) and production (Bogard et al., 2014; Donis et al., 2017). No temporal or spatial (branches versus main basin) differences in net metabolic CH₄ rate were detected due to a high variability and limited data points.

3.7 Ecosystem scale GHG budgets

Estimated sources / sinks of CO₂ and CH₄ were collated into a budget to evaluate their relative impact on epilimnetic gas concentration and to assess whether their sum matches the measured surface gas fluxes in each section of the reservoir. Fig. 3 depicts such reconstruction of the epilimnetic CO₂ and CH₄ budgets in Batang Ai, as well as the uncertainty limits of each component. While each process varied in time, their relative importance in driving surface fluxes was generally similar from one sampling campaign to another (Table S2 and S3).

345 3.7.1 CO₂ budget

For CO₂, epilimnetic sediment inputs had a small contribution, being typically an order of magnitude lower than measured surface fluxes in both sections of the reservoir (Fig. 3a, b and Table S2). Vertical CO₂ inputs from lower depths on the other hand contributed substantially to surface fluxes in the branches and especially in the main basin (mean of 0.7 and 4.5 mmol m⁻² d⁻¹ respectively, Fig. 3a, b and Table S2), indicating that hypolimnetic processes impact surface emissions despite the permanent stratification. Horizontal inputs of CO₂ averaged 4.3 mmol m⁻² d⁻¹ in the branches, however, they decreased by an order of magnitude when reaching the main basin (mean of 0.3 mmol m⁻² d⁻¹). Thus, direct CO₂ inputs from the inflows notably increase surface flux rates in the reservoir branches but only minimally in the main basin. Net CO₂ metabolism was surprisingly variable (switching from negative to positive NEP on a daily time scale), thus making it difficult to derive a sufficiently precise ecosystem-scale estimate to close the epilimnetic budget (Fig. 3a, b), despite high sampling resolution (n = 66 daily metabolic rates). Including the metabolism substantially shifts the mean of the CO₂ epilimnetic budget (sum of sources and sinks) to a negative value and drastically increases its uncertainty (Fig. 3a, b and Table S2), reflecting a potentially important but poorly resolved role of metabolism in the budget because of its variability. However, given that metabolism acts more likely as a CO₂ sink on average, our best assessment suggests that, vertical transport from deeper layers is the main source sustaining surface CO₂ out-flux in the main basin of Batang Ai.

360 3.7.2 CH₄ budget

In contrast with CO₂, vertical transport was the smallest source of CH₄ to the epilimnion, contributing to only 2 % of surface fluxes in both reservoir sections (Fig. 3c, d and Table S3). In the branches, sediment inputs and net CH₄ metabolic rates were both relatively low (mean of 0.04 ± 0.02 and 0.04 ± 0.05 mmol m⁻² d⁻¹) and had little impact on the budget, corresponding each to 4 % of surface fluxes in that section (Fig. 3c and Table S3). On the other hand, horizontal inputs were the dominant and most variable source sustaining CH₄ emissions in the branches, where the epilimnetic mass balance closed almost perfectly (Fig. 3c and Table S3). Despite being the main CH₄ source in the branches, horizontal transport was a negligible component in the main basin (1 % of the flux, Fig. 3d and Table S3). Instead, sediment inputs played a larger role in that section, with a mean of 0.10 (± 0.06) mmol m⁻² d⁻¹, fueling 23 % of surface emissions in the main basin (Fig. 3d and Table S3). As with CO₂, the most variable CH₄ component of the mass balance in the main basin was the net metabolism within the epilimnion (mean of -0.16 ± 0.19 mmol m⁻² d⁻¹). Considering all sources, the CH₄ budget indicates a deficit of 0.34 mmol m⁻² d⁻¹ to explain measured surface emissions in the main basin (Fig. 3d and Table S3).

4 Discussion

Our results have highlighted both the importance and the challenges associated with quantifying simultaneously all the components of the epilimnetic CO₂ and CH₄ budgets, particularly in a hydrologically complex reservoir system. While mass fluxes (hydrological, sedimentary, and air-water fluxes) are relatively easy to constrain, internal C processing, namely the net

metabolic balances between production and consumption of CO₂ and CH₄ are highly dynamic in both time and space, leading to significant uncertainties when extrapolated to the ecosystem scale. In many studies, some components are only inferred by difference. While convenient from a mass-balance perspective, we argue that assessing all components together is necessary to clearly identify knowledge gaps as well as sources of uncertainty.

380 4.1 Spatial dynamics of CO₂ and CH₄

The decrease in gas concentration and air-water fluxes along the hydrological continuum observed across sampling campaigns and for both CH₄ and CO₂ reflects a robust spatial structure of the gases. Concurrently, estimates of the horizontal GHG inputs shows a clear and consistent spatial pattern, being high in the branches but negligible in the main basin. A temporal effect of riverine inputs was also observed as the two sampling campaigns with the highest horizontal CH₄ inputs coincided with the
385 highest CH₄ emissions in the branches (Table S3). All these results concord with a progressively reduced influence of direct GHG catchment inputs and greater preponderance of internal processes along the hydrological continuum as observed in river networks (Hotchkiss et al., 2015) and in lakes and reservoirs (Chmiel et al., 2020; Loken et al., 2019; Paranaíba et al., 2018; Pasche et al., 2019).

For CO₂, the sharpest change in surface metrics (concentration, flux, and isotopic signature) was observed between the inflows and the reservoir branches (Fig. 2a, b, c). Despite large riverine inputs (Table S2), the branches exhibited low CO₂
390 concentration and fluxes, as well as an increase in δ¹³C<sub>CO₂ matching with high GPP values (Fig. 2a, b, c and 4a). This may reflect increased light availability for phytoplankton when transitioning from the turbid inflows to the reservoir branches (higher Secchi depth, Table 1), a pattern previously reported in other reservoirs (Kimmel and Groeger, 1984; Pacheco et al., 2015; Thornton et al., 1990). While the branch areas are often associated with high CO₂ outflux due to riverine inputs (Beaulieu
395 et al., 2016; Paranaíba et al., 2018; Pasche et al., 2019; Roland et al., 2010; Rudorff et al., 2011), they are occasionally observed to have low air-water flux due to simultaneous nutrient inputs (Loken et al., 2019; Paranaíba et al., 2018; Wilkinson et al., 2016). In Batang Ai, inflows have a high nutrients (TP and TN) to DOC ratio compared to the reservoir branches (Table 1), providing higher inputs of nutrients relative to organic matter, and thus likely stimulating primary production more than respiration. This hypothesis is consistent with a higher GPP: ER ratio and mean Chl_a concentrations measured in the branches
400 compared to the main basin (Fig. 4a and Table 1). The variability of CO₂ concentration within the reservoir (branches and main basin) was negatively correlated to temperature, likely due to its effect on GPP (Bogard et al., 2020). This further highlights the important role of primary production in modulating CO₂ dynamics throughout the reservoir, and particularly in the branches.</sub>

The correlation between surface CH₄ and TN in the reservoir suggests that primary production may also affect CH₄ dynamics.
405 Nutrient content was shown in previous studies to enhance CH₄ production in the sediments (Beaulieu et al., 2019; Gebert et al., 2006; Isidorova et al., 2019) and in the oxic water column (Bogard et al., 2014), through its link with algal production and decomposition. However, CH₄ concentration and flux variability were strongly driven by a spatial / hydrological structure, gradually decreasing from the inflows to the main basin. This likely reflects the combined effect of terrestrial inputs and a

decreasing contact of water with sediments along the water channel. Surface $\delta^{13}\text{CH}_4$ signatures varied substantially but without
410 a consistent spatial pattern (Fig. 2f), indicating that the surface CH_4 pool is shaped by multiple sources / processes (metabolism,
riverine, and sediment inputs) varying through space and time.

The changing relative contribution of sources and processes shaping surface CO_2 and CH_4 concentrations varies with the
system hydro-morphology, from the inflows to the main reservoir basin, and lead to a progressive decoupling between the two
gases along the continuum (Fig. S2). The observed CO_2 and CH_4 coupling in the inflows and branches is associated to a
415 common catchment source, as previously reported in other systems including soil-water (Lupon et al., 2019), streams (Rasilo
et al., 2017), and lake and reservoir inflow areas (Loken et al., 2019; Natchimuthu et al., 2017; Paranaíba et al., 2018). Indeed,
horizontal inputs are the main source of both CO_2 and CH_4 in the upstream reaches of Batang Ai, accounting on average for
91 and 92 % of their respective surface out-flux in the branch section (Fig. 3a, c and Tables S2 and S3). The hydro-
morphometry of these channels can explain the large impact of horizontal inputs in the branch section, which is characterized
420 by a relatively small ratio of water to catchment area and a direct connection to the major river inflows creating a strong link
between the catchment and the branches. However, when reaching the main basin, this link weakens due to a longer distance
from river inflows and the dilution of horizontal inputs in a larger water volume. Thus, in the main basin, CO_2 and CH_4 are
mostly driven by internal sources, diverging between the two gases, with vertical inputs from the bottom layer supporting on
average 60 % of CO_2 compared to 2 % of CH_4 fluxes, while sediment inputs sustained 7 versus 23 % of CO_2 and CH_4 fluxes
425 respectively in that section. This decoupling partly results from the two gases having distinct metabolic pathways: mainly
aerobic for CO_2 and anaerobic for CH_4 , leading to their sources and sinks being spatially disconnected in the main basin.
Consequently, sediments being a mostly anaerobic environment are a more important source of CH_4 relative to CO_2 , while the
metalimnetic layer being oxic-hypoxic acts as a sink of CH_4 and source of CO_2 via aerobic CH_4 oxidation (Fig. S4). Overall,
the spatial patterns reported here highlight the hydrodynamic zonation common in reservoirs and its diverging effect on CO_2
430 versus CH_4 cycling.

4.2 CO_2 metabolism

Our observation that GPP often exceeded ER (Fig. 4a) was not unexpected given the very low DOC concentration ($< 1 \text{ mg L}^{-1}$).
Previous work has reported that $\text{DOC} > 4 \text{ mg L}^{-1}$ is required to sustain persistent net heterotrophy and CO_2 evasion (Hanson
et al., 2003; Prairie et al., 2002). Throughout the reservoir, we found high day-to-day variability in both ER and GPP, but with
435 no apparent link to weather data (light and rain, data not shown). The absence of such a link at a daily time scale has been
previously reported (Coloso et al., 2011), while other studies associated daily variations in metabolism with changes in water
inflows carrying nutrients (Pacheco et al., 2015; Staehr and Sand-Jensen, 2007), or thermocline stability regulating
hypolimnetic water incursions to the epilimnion (Coloso et al., 2011). Such variations in thermocline depth are thought to be
more common in warm tropical systems (Lewis, 2010), and were observed across sampling campaigns in Batang Ai, especially
440 in the branches where the depth of the mixed layer varied considerably ($\text{SD} = 2.3 \text{ m}$, Table 1). Hence, hydrological and physical
factors may regulate spatial and daily patterns of GPP and ER rates in Batang Ai through their influence on nutrient dynamics.

The accuracy of rates derived from diel O₂ monitoring partly depends on the respiratory and photosynthetic quotients (RQ and PQ) assumed for the conversion of metabolic rates from O₂ to CO₂. A quotient differing from the assumed 1:1 ratio can lead to an under or over-estimation of net CO₂ production. The fact that net CO₂ metabolic rates were on average higher in incubations, based on direct CO₂ measurements compared to diel O₂ monitoring (Fig. 4b and Table S2), hints at a deviation of the metabolic quotients from unity in Batang Ai. Additionally, surface O₂ versus CO₂ concentrations shows that the departure of these gases from saturation varies widely around the expected 1:-1 line, with many surface samples oversaturated in both O₂ and CO₂, especially in the branches (Fig. 5). This indicates an excess O₂ and / or CO₂ that can be due to a PQ and / or a RQ higher than 1, or to external CO₂ inputs to the epilimnion (Vachon et al., 2020), for instance from the inflows or the bottom layer (Table S2). Metabolic quotients have been shown to vary widely, depending on the type and magnitude of photochemical and biological reactions at play (Berggren et al., 2012; Lefèvre and Merlivat, 2012; Vachon et al., 2020; Williams and Robertson, 1991). For instance, CH₄ oxidation and production, evidently occurring in Batang Ai's epilimnion (Table S2 and S3), diverge from the metabolic O₂:CO₂ ratio of one, with CH₄ oxidation consuming two moles of O₂ for each mole of CO₂ produced, and acetoclastic methanogenesis producing CO₂ without O₂ consumption. Even though net CH₄ processing rates are a minor portion of the epilimnetic C cycling in Batang Ai (1-2 orders of magnitudes lower than CO₂ metabolic rates, Tables S2 and S3), these reactions (and other unmeasured processes) have the potential to alter the O₂:CO₂ metabolic quotient at an ecosystem scale. The lack of direct measure of metabolic quotients in Batang Ai adds uncertainty to the net CO₂ metabolism estimates based on O₂ data. The observed decoupling of O₂ and CO₂ metabolism in Batang Ai highlights the need for a deeper understanding of the biochemical reactions occurring in the epilimnion, and their effect on metabolic quotients.

Overall, our results from Batang Ai reservoir point to water column metabolism as both a key process in the CO₂ epilimnetic budget and a challenging one to estimate at an ecosystem scale (Fig. 3a, b). Improving this requires a better mechanistic knowledge of the physical and biochemical processes at play and how they interact to shape NEP.

4.3 CH₄ metabolism

Incubation results exhibited a wide range of net CH₄ metabolism: from net oxidation to net production. CH₄ oxidation is known to be highly dependent on CH₄ availability and is optimal in low oxygen and low light conditions (Borrel et al., 2011; Thottathil et al., 2018, 2019), whereas CH₄ production in the oxic water is still poorly understood but have been frequently linked to phytoplankton growth (Berg et al., 2014; Bogard et al., 2014; Lenhart et al., 2015; Wang et al., 2017). A large variability in results exists among the studies that have assessed the net balance of CH₄ metabolism in the water column, with some studies reporting pelagic CH₄ production as a largely dominant process (Donis et al., 2017) while others find no trace of it (Bastviken et al., 2008). Based on spatial patterns of surface CH₄ concentration and isotopic signature with distance to shore, DelSontro et al. (2018b) showed that, in 30 % of their studied temperate lakes, CH₄ oxidation was dominant versus 70 % dominated by net pelagic production. In Batang Ai, surface $\delta^{13}\text{C}_{\text{CH}_4}$ values were highly variable (-82.5 to -47.7 ‰) but mostly uncorrelated with distance to shore, except a positive correlation indicative of oxidation in the Nov-Dec 2016 ($R^2_{\text{adj}} = 0.29$, p-value = 0.01,

475 Fig. 6b) coinciding with a strong inverse pattern for CH₄ concentration ($R^2_{adj} = 0.54$, p-value < 0.001, Fig. 6a). This suggests
a temporal shift in processes driving surface CH₄ patterns. Also, some measured surface $\delta^{13}\text{CH}_4$ values were lower than the
mean $\delta^{13}\text{CH}_4$ from the sediments (-66.0 ‰, unpublished data), suggesting another highly depleted source of pelagic CH₄ in the
system. This is in line with water incubation results often showing positive net CH₄ production (Table S3). When reported as
mean areal rates, CH₄ metabolism ranged from net consumption to net production of CH₄ (-0.29 to 0.94 mmol.m⁻².d⁻¹), which
480 reflects its potential in having a high impact, either positive or negative, on the epilimnetic CH₄ budget at the reservoir scale
(Fig. 3d and Table S3). Results in Batang Ai show that the net balance of CH₄ metabolic processes varies widely even within
a single system. However, the factors regulating this balance remain largely unknown. Investigating such factors constitute a
key step in resolving CH₄ budgets in lakes and reservoirs.

4.4 Epilimnetic GHG budgets

485 For CO₂, measured surface fluxes in both reservoir sections fall in the range of possible values estimated by the sum of
epilimnetic processes and their uncertainties (Fig. 3a, b and Table S2). However, the averages of those two terms differ
substantially, due to negative values of metabolism shifting the mean of the mass balance towards net CO₂ consumption
whereas, on average, surface out-flux was measured from the reservoir. This discrepancy indicates either a missing source of
CO₂ in the budget or the underestimation of one of the processes. While lateral groundwater input is a potential source not
490 explicitly considered, it is probably modest given the small ratio of littoral area to epilimnion volume, and is unlikely to account
for the large CO₂ deficit in the budget. On the other hand, underestimation of the CO₂ metabolic balance is much more likely,
given its large variability and uncertainty around its mean value. Additionally, a systematic underestimation of the CO₂
metabolic rates derived from the diel O₂ method is very possible in Batang Ai given the likely deviation of metabolic quotients
around the 1:1 line. As an example, when setting the photosynthetic quotient to 1.2 instead of 1, which remains well within
495 the literature range (Lefèvre and Merlivat, 2012; Williams and Robertson, 1991), the average epilimnetic CO₂ mass balance
would increase from -17.7 to 4.3 mmol m⁻² d⁻¹ in the branches and from -6.5 to 6.2 mmol m⁻² d⁻¹ in the main basin, closely
matching measured surface fluxes of 4.7 and 7.5 mmol m⁻² d⁻¹ in the respective sections. Thus, constraining the metabolic
component, especially the O₂: CO₂ quotients, is key for closing the CO₂ epilimnetic budget. Another way to decipher the role
of metabolism, given its high uncertainty, is by difference in a mass balance exercise. Assuming mean estimates of all other
500 components are accurate, CO₂ net metabolic rates would have to be equal to -0.8 and 2.1 mmol m⁻² d⁻¹ in the branches and
main basin respectively for the mass balance to close. This corresponds to a contribution of -18 and 28 % to the surface CO₂
flux in the respective sections (Fig. 3a, b), suggesting a substantial impact of metabolism on the CO₂ epilimnetic budget.

In the case of CH₄, the measured epilimnetic budget in the branches is surprisingly close to the observed surface flux, largely
fueled by horizontal inputs. Hence, CH₄ emissions from the branches reflect catchment CH₄ loads rather than internal
505 processes. However, in the main basin, these inputs become negligible and the estimated budget does not match measured
emissions, indicating a deficit of 0.49 mmolCH₄ m⁻² d⁻¹. This amount cannot be explained by a potential underestimation of
horizontal or vertical inputs since they are two orders of magnitude lower. Similarly, sediment inputs would need to be six

time higher than estimated to fulfill the budget deficit, which is unlikely given their much lower range of uncertainty. Thus, the most plausible source to close the mass balance in the main basin would be water column CH₄ production. Although the estimated CH₄ metabolism indicates an average net consumption rather than a net production (-0.16 mmol m⁻² d⁻¹), this mean value is based on only 3 data points and has a high uncertainty associated to it (SE = 0.19 mmol m⁻² d⁻¹, Table S3). Closing the mass balance would require a net volumetric CH₄ production of about 0.03 μmol L⁻¹ d⁻¹ in the water column of the main basin. This value seems plausible since an equal production rate was measured in one of the incubations, and it is at the low end of the range reported in other systems (Bogard *et al.*, 2014 ; DelSontro *et al.*, 2018b ; Donis *et al.*, 2017). This mass balance approach suggests that water column metabolism could be the dominant source of CH₄ in the main basin of Batang Ai, potentially sustaining up to 75 % of surface emissions in that reservoir section (Fig. 3d). Even though this deductive approach is an indirect assessment of water column CH₄ metabolism, it emphasizes its likely key role in the reservoir epilimnetic CH₄ budget, while measured metabolic rates highlight the wide variability of this process and the need for more intensive research into its controls at spatial and temporal scales.

The combination of empirical and mass balance approaches in this study provide not only a partitioning of the contribution of each source / sink in sustaining surface CO₂ and CH₄ fluxes, but also a clear picture of the uncertainties and challenges associated to the estimation of each component.

5 Conclusion

The estimated epilimnetic CO₂ and CH₄ budgets in Batang Ai has helped define the role of different processes in shaping the reservoir surface GHG fluxes to the atmosphere. Results showed that horizontal riverine inputs are important sources of GHG in the reservoir branches (especially for CH₄). This creates a coupling between CO₂ and CH₄ close to the river deltas, which gradually fades along the water flow, until the surface concentrations of the two gases become completely uncoupled in the main basin being driven by different sources. For instance, vertical inputs from the bottom layer contributed significantly to surface CO₂ saturation, while being negligible in the case of CH₄ due to metalimnetic oxidation. Inversely, sediment inputs played a notably greater role in sustaining epilimnetic oversaturation of CH₄ compared to CO₂ in the main basin. Nonetheless, the epilimnetic budgets of both gases presented a high sensitivity to water column metabolism. This result is likely representative of large systems with a high volume of water versus sediments, which is common for hydroelectric reservoirs. However, metabolic balances of CO₂ and CH₄ were extremely variable in space and time, switching from a net production to a net consumption of the gases, and leading to highly uncertain ecosystem-scale estimates, which emphasizes the key but unconstrained role of metabolism in the overall GHG budgets. Factors driving these metabolic changes are not well defined based on current knowledge, highlighting the need for further research on the subject. Overall, this study gives an integrative portrait of the relative contribution of different sources to surface CO₂ and CH₄ fluxes in a permanently stratified reservoir including its transition zones (branches). Conclusions and insights derived from this work likely reflect C dynamics in other

540 similar systems, and highlight knowledge gaps guiding future research to better understand and predict aquatic GHG fluxes and regulation.

Author contribution

CS contributed to conceptualization, methodology, validation, formal analysis, investigation, data curation, writing - original draft, writing – review and editing, and project administration. YTP contributed to Methodology, validation, investigation, 545 resources, writing – review and editing, supervision, and funding acquisition.

Competing interests

The authors declare that they have no conflict of interest.

Acknowledgments

This work was funded by Sarawak Energy Berhad and the Natural Science and Engineering Research Council of Canada 550 (Discovery grant to Y.T.P. and BES-D scholarship to C.S.). We are grateful to Karen Lee Suan Ping and Jenny Choo Cheng Yi for their logistic support and participation in sampling campaigns. We also thank Jessica Fong Fung Yee, Amar Ma'aruf Bin Ismawi, Gerald Tawie Anak Thomas, Hilton Bin John, Paula Reis, Sara Mercier-Blais and Karelle Desrosiers for their help on the field, and Katherine Velghe and Marilyne Robidoux for their assistance during laboratory analyses.

References

- Adams, D. D.: Diffuse Flux of Greenhouse Gases — Methane and Carbon Dioxide — at the Sediment-Water Interface of Some Lakes and Reservoirs of the World, in *Greenhouse Gas Emissions - Fluxes and Processes*, pp. 129–153., 2005.
- Algesten, G., Sobek, S., Bergström, A. K., Jonsson, A., Tranvik, L. J. and Jansson, M.: Contribution of sediment respiration to summer CO₂ emission from low productive boreal and subarctic lakes, *Microb. Ecol.*, 50(4), 529–535, doi:10.1007/s00248- 560 005-5007-x, 2005.
- Appling, A. P., Hall, R. O., Arroita, M. and Yackulic, C. B.: *StreamMetabolizer: Models for Estimating Aquatic Photosynthesis and Respiration*, [online] Available from: <https://github.com/USGS-R/streamMetabolizer>, 2018.
- Barrette, N. and Laprise, R.: A One-Dimensional Model for Simulating the Vertical Transport of Dissolved CO₂ and CH₄ in Hydroelectric Reservoirs, in *Greenhouse Gas Emissions - Fluxes and Processes*, pp. 575–595., 2005.

- 565 Barros, N., Cole, J. J., Tranvik, L. J., Prairie, Y. T., Bastviken, D., Huszar, V. L. M., del Giorgio, P. and Roland, F.: Carbon emission from hydroelectric reservoirs linked to reservoir age and latitude, *Nat. Geosci.*, 4(9), 593–596, doi:10.1038/ngeo1211, 2011.
- Bastviken, D., Cole, J. J., Pace, M. L. and Van de-Bogert, M. C.: Fates of methane from different lake habitats: Connecting whole-lake budgets and CH₄ emissions, *J. Geophys. Res. Biogeosciences*, 113(2), 1–13, doi:10.1029/2007JG000608, 2008.
- 570 Bastviken, D., Tranvik, L. J., Downing, J. A., Crill, P. M. and Enrich-Prast, A.: Freshwater Methane Emissions Offset the Continental Carbon Sink, *Science* (80-.), 331(6013), 50–50, doi:10.1126/science.1196808, 2011.
- Beaulieu, J. J., McManus, M. G. and Nietch, C. T.: Estimates of reservoir methane emissions based on a spatially balanced probabilistic-survey, *Limnol. Oceanogr.*, 61(S1), S27–S40, doi:10.1002/lno.10284, 2016.
- 575 Beaulieu, J. J., DelSontro, T. and Downing, J. A.: Eutrophication will increase methane emissions from lakes and impoundments during the 21st century, *Nat. Commun.*, 10(1), 3–7, doi:10.1038/s41467-019-09100-5, 2019.
- Berg, A., Lindblad, P. and Svensson, B. H.: Cyanobacteria as a source of hydrogen for methane formation, *World J. Microbiol. Biotechnol.*, 30(2), 539–545, doi:10.1007/s11274-013-1463-5, 2014.
- Berggren, M., Lapierre, J.-F. and del Giorgio, P. A.: Magnitude and regulation of bacterioplankton respiratory quotient across freshwater environmental gradients, *ISME J.*, 6(5), 984–993, doi:10.1038/ismej.2011.157, 2012.
- 580 Bižić, M., Klintzsch, T., Ionescu, D., Hindyieh, M., Guentzel, M., Muro-Pastor, A. M., Eckert, W., Urich, T., Keppler, F. and Grossart, H.-P.: Aquatic and terrestrial Cyanobacteria produce methane, *Sci. Adv.*, (13), In Press, 2019.
- Blais, J. M. and Kalff, J.: The influence of lake morphometry on sediment focusing, *Limnol. Oceanogr.*, 40(3), 582–588, doi:10.4319/lo.1995.40.3.0582, 1995.
- 585 Bogard, M. J. and del Giorgio, P. A.: The role of metabolism in modulating CO₂ fluxes in boreal lakes, *Global Biogeochem. Cycles*, 30(10), 1509–1525, doi:10.1002/2016GB005463, 2016.
- Bogard, M. J., del Giorgio, P. a, Boutet, L., Chaves, M. C. G., Prairie, Y. T., Merante, A. and Derry, A. M.: Oxidic water column methanogenesis as a major component of aquatic CH₄ fluxes., *Nat. Commun.*, 5(May), 5350, doi:10.1038/ncomms6350, 2014.
- Bogard, M. J., St-Gelais, N. F., Vachon, D. and del Giorgio, P. A.: Patterns of Spring/Summer Open-Water Metabolism Across Boreal Lakes, *Ecosystems*, doi:10.1007/s10021-020-00487-7, 2020.

- 590 Borrel, G., Jézéquel, D., Biderre-Petit, C., Morel-Desrosiers, N., Morel, J. P., Peyret, P., Fonty, G. and Lehours, A. C.: Production and consumption of methane in freshwater lake ecosystems, *Res. Microbiol.*, 162(9), 832–847, doi:10.1016/j.resmic.2011.06.004, 2011.
- Chmiel, H. E., Hofmann, H., Sobek, S., Efremova, T. and Pasche, N.: Where does the river end? Drivers of spatiotemporal variability in CO₂ concentration and flux in the inflow area of a large boreal lake, *Limnol. Oceanogr.*, 65(6), 1161–1174, 595 doi:10.1002/lno.11378, 2020.
- Coloso, J. J., Cole, J. J. and Pace, M. L.: Difficulty in Discerning Drivers of Lake Ecosystem Metabolism with High-Frequency Data, *Ecosystems*, 14(6), 935–948, doi:10.1007/s10021-011-9455-5, 2011.
- Conrad, R.: The global methane cycle: recent advances in understanding the microbial processes involved, *Environ. Microbiol. Rep.*, 1(5), 285–292, doi:10.1111/j.1758-2229.2009.00038.x, 2009.
- 600 Deemer, B. R., Harrison, J. A., Li, S., Beaulieu, J. J., DelSontro, T., Barros, N., Bezerra-Neto, J. F., Powers, S. M., dos Santos, M. A. and Vonk, J. A.: Greenhouse Gas Emissions from Reservoir Water Surfaces: A New Global Synthesis, *Bioscience*, 66(11), 949–964, doi:10.1093/biosci/biw117, 2016.
- DelSontro, T., Beaulieu, J. J. and Downing, J. A.: Greenhouse gas emissions from lakes and impoundments: Upscaling in the face of global change, *Limnol. Oceanogr. Lett.*, 3(3), 64–75, doi:10.1002/lol2.10073, 2018a.
- 605 DelSontro, T., del Giorgio, P. A. and Prairie, Y. T.: No Longer a Paradox: The Interaction Between Physical Transport and Biological Processes Explains the Spatial Distribution of Surface Water Methane Within and Across Lakes, *Ecosystems*, 21(6), 1073–1087, doi:10.1007/s10021-017-0205-1, 2018b.
- Donis, D., Flury, S., Stöckli, A., Spangenberg, J. E., Vachon, D. and McGinnis, D. F.: Full-scale evaluation of methane production under oxic conditions in a mesotrophic lake, *Nat. Commun.*, 8(1), 1–11, doi:10.1038/s41467-017-01648-4, 2017.
- 610 Encinas Fernández, J., Peeters, F. and Hofmann, H.: Importance of the autumn overturn and anoxic conditions in the hypolimnion for the annual methane emissions from a temperate lake, *Environ. Sci. Technol.*, 48(13), 7297–7304, doi:10.1021/es4056164, 2014.
- Ferland, M. E., Prairie, Y. T., Teodoru, C. and Del Giorgio, P. A.: Linking organic carbon sedimentation, burial efficiency, and long-term accumulation in boreal lakes, *J. Geophys. Res. Biogeosciences*, 119(5), 836–847, doi:10.1002/2013JG002345, 615 2014.
- Gebert, J., Köthe, H. and Gröngroft, A.: Prognosis of methane formation by river sediments, *J. Soils Sediments*, 6(2), 75–83, doi:10.1065/jss2006.04.153, 2006.

- 620 Gruca-Rokosz, R. and Tomaszek, J. A.: Methane and carbon dioxide in the sediment of a eutrophic reservoir: Production pathways and diffusion fluxes at the sediment-water interface, *Water, Air, Soil Pollut.*, 226(2), doi:10.1007/s11270-014-2268-3, 2015.
- Guérin, F. and Abril, G.: Significance of pelagic aerobic methane oxidation in the methane and carbon budget of a tropical reservoir, *J. Geophys. Res. Biogeosciences*, 112(G3), n/a–n/a, doi:10.1029/2006JG000393, 2007.
- 625 Guérin, F., Deshmukh, C., Labat, D., Pighini, S., Vongkhamsao, A., Guédant, P., Rode, W., Godon, A., Chanudet, V., Descloux, S. and Serça, D.: Effect of sporadic destratification, seasonal overturn, and artificial mixing on CH₄ emissions from a subtropical hydroelectric reservoir, *Biogeosciences*, 13(12), 3647–3663, doi:10.5194/bg-13-3647-2016, 2016.
- Hall, R. O. and Hotchkiss, E. R.: Stream Metabolism, in *Methods in Stream Ecology*, vol. 2, pp. 219–233, Elsevier., 2017.
- Hanson, P. C., Bade, D. L., Carpenter, S. R. and Kratz, T. K.: Lake metabolism: Relationships with dissolved organic carbon and phosphorus, *Limnol. Oceanogr.*, 48(3), 1112–1119, doi:10.4319/lo.2003.48.3.1112, 2003.
- 630 Hotchkiss, E. R., Hall Jr, R. O., Sponseller, R. A., Butman, D., Klaminder, J., Laudon, H., Rosvall, M. and Karlsson, J.: Sources of and processes controlling CO₂ emissions change with the size of streams and rivers, *Nat. Geosci.*, 8(9), 696–699, doi:10.1038/ngeo2507, 2015.
- Huttunen, J. T., Väisänen, T. S., Hellsten, S. K. and Martikainen, P. J.: Methane fluxes at the sediment-water interface in some boreal lakes and reservoirs, *Boreal Environ. Res.*, 11(1), 27–34, 2006.
- 635 Imboden, D. M.: Limnologische Transport- und Nährstoffmodelle, *Schweizerische Zeitschrift für Hydrol.*, 35(1), 29–68, doi:10.1007/BF02502063, 1973.
- International Hydropower Association (IHA): GHG measurement guidelines for freshwater reservoirs., 2010.
- Isidorova, A., Grasset, C., Mendonça, R. and Sobek, S.: Methane formation in tropical reservoirs predicted from sediment age and nitrogen, *Sci. Rep.*, 9(1), 1–9, doi:10.1038/s41598-019-47346-7, 2019.
- 640 Kankaala, P., Huotari, J., Tulonen, T. and Ojala, A.: Lake-size dependent physical forcing drives carbon dioxide and methane effluxes from lakes in a boreal landscape, *Limnol. Oceanogr.*, 58(6), 1915–1930, doi:10.4319/lo.2013.58.6.1915, 2013.
- Karlsson, J., Jansson, M. and Jonsson, A.: Respiration of allochthonous organic carbon in unproductive forest lakes determined by the Keeling plot method, *Limnol. Oceanogr.*, 52(2), 603–608, doi:10.4319/lo.2007.52.2.0603, 2007.

- 645 Kim, B., Choi, K., Kim, C., Lee, U. H. and Kim, Y. H.: Effects of the summer monsoon on the distribution and loading of organic carbon in a deep reservoir, Lake Soyang, Korea, *Water Res.*, 34(14), 3495–3504, doi:10.1016/S0043-1354(00)00104-4, 2000.
- Kimmel, B. L. and Groeger, A. W.: Factors Controlling Primary Production in Lakes and Reservoirs: a Perspective, *Lake Reserv. Manag.*, 1(1), 277–281, doi:10.1080/07438148409354524, 1984.
- 650 Kindler, R., Siemens, J., Kaiser, K., Walmsley, D. C., Bernhofer, C., Buchmann, N., Cellier, P., Eugster, W., Gleixner, G., Grunwald, T., Heim, A., Ibrom, A., Jones, S. K., Jones, M., Klumpp, K., Kutsch, W., Larsen, K. S., Lehuger, S., Loubet, B., Mckenzie, R., Moors, E., Osborne, B., Pilegaard, K., Rebmann, C., Saunders, M., Schmidt, M. W. I., Schrupf, M., Seyfferth, J., Skiba, U., Soussana, J. F., Sutton, M. A., Tefs, C., Vowinckel, B., Zeeman, M. J. and Kaupenjohann, M.: Dissolved carbon leaching from soil is a crucial component of the net ecosystem carbon balance, *Glob. Chang. Biol.*, 17(2), 1167–1185, doi:10.1111/j.1365-2486.2010.02282.x, 2011.
- 655 Kreling, J., Bravidor, J., McGinnis, D. F., Koschorreck, M. and Lorke, A.: Physical controls of oxygen fluxes at pelagic and benthic oxyclines in a lake, *Limnol. Oceanogr.*, 59(5), 1637–1650, doi:10.4319/lo.2014.59.5.1637, 2014.
- Lefèvre, N. and Merlivat, L.: Carbon and oxygen net community production in the eastern tropical Atlantic estimated from a moored buoy, *Global Biogeochem. Cycles*, 26(1), n/a–n/a, doi:10.1029/2010GB004018, 2012.
- 660 Lenhart, K., Klintzsch, T., Langer, G., Nehrke, G., Bunge, M., Schnell, S. and Keppler, F.: Evidence for methane production by marine algae (*Emiliana huxleyi*) and its implication for the methane paradox in oxic waters, *Biogeosciences Discuss.*, 12(24), 20323–20360, doi:10.5194/bgd-12-20323-2015, 2015.
- Lewis, W. M.: Biogeochemistry of tropical lakes, *SIL Proceedings*, 1922-2010, 30(10), 1595–1603, doi:10.1080/03680770.2009.11902383, 2010.
- Li, M., Peng, C., Wang, M., Xue, W., Zhang, K., Wang, K., Shi, G. and Zhu, Q.: The carbon flux of global rivers: A re-evaluation of amount and spatial patterns, *Ecol. Indic.*, 80(April), 40–51, doi:10.1016/j.ecolind.2017.04.049, 2017.
- 665 Loken, L. C., Crawford, J. T., Schramm, P. J., Stadler, P., Desai, A. R. and Stanley, E. H.: Large Spatial and Temporal Variability of Carbon Dioxide and Methane in a Eutrophic Lake, *J. Geophys. Res. Biogeosciences*, 124(7), 2248–2266, doi:10.1029/2019JG005186, 2019.
- 670 St. Louis, V. L., Kelly, C. A., Duchemin, É., Rudd, J. W. M. and Rosenberg, D. M.: Reservoir Surfaces as Sources of Greenhouse Gases to the Atmosphere: A Global Estimate, *Bioscience*, 50(9), 766–775, doi:10.1641/0006-3568(2000)050[0766:RSASOG]2.0.CO;2, 2000.
- Lupon, A., Denfeld, B. A., Laudon, H., Leach, J., Karlsson, J. and Sponseller, R. A.: Groundwater inflows control patterns and sources of greenhouse gas emissions from streams, *Limnol. Oceanogr.*, 64(4), 1545–1557, doi:10.1002/lno.11134, 2019.

- Maavara, T., Lauerwald, R., Regnier, P. and Van Cappellen, P.: Global perturbation of organic carbon cycling by river damming, *Nat. Commun.*, 8(May), 1–10, doi:10.1038/ncomms15347, 2017.
- 675 Martinsen, K. T., Kragh, T. and Sand-Jensen, K.: Carbon dioxide efflux and ecosystem metabolism of small forest lakes, *Aquat. Sci.*, 82(1), 9, doi:10.1007/s00027-019-0682-8, 2020.
- Monteith, D. T., Stoddard, J. L., Evans, C. D., De Wit, H. A., Forsius, M., Høgåsen, T., Wilander, A., Skjelkvåle, B. L., Jeffries, D. S., Vuorenmaa, J., Keller, B., Kopécek, J. and Vesely, J.: Dissolved organic carbon trends resulting from changes in atmospheric deposition chemistry, *Nature*, 450(7169), 537–540, doi:10.1038/nature06316, 2007.
- 680 Natchimuthu, S., Sundgren, I., Gålfalk, M., Klemetsson, L. and Bastviken, D.: Spatiotemporal variability of lake pCO₂ and CO₂ fluxes in a hemiboreal catchment, *J. Geophys. Res. Biogeosciences*, 122(1), 30–49, doi:10.1002/2016JG003449, 2017.
- Oahey, N. S.: Determination of the Rate of Dissipation of Turbulent Energy from Simultaneous Temperature and Velocity Shear Microstructure Measurements, *J. Phys. Oceanogr.*, 12(3), 256–271, doi:10.1175/1520-0485(1982)012<0256:DOTROD>2.0.CO;2, 1982, 1982.
- 685 Odum, H. T.: Primary Production in Flowing Waters¹, *Limnol. Oceanogr.*, 1(2), 102–117, doi:10.4319/lo.1956.1.2.0102, 1956.
- Osborn, T. R.: Estimates of the Local Rate of Vertical Diffusion from Dissipation Measurements, *J. Phys. Oceanogr.*, 10(1), 83–89, doi:10.1175/1520-0485(1980)010<0083:EOTLRO>2.0.CO;2, 1980.
- 690 Pace, M. L. and Prairie, Y. T.: Respiration in lakes, in *Respiration in Aquatic Ecosystems*, pp. 103–121, Oxford University Press., 2005.
- Pacheco, F. S., Soares, M. C. S., Assireu, A. T., Curtarelli, M. P., Roland, F., Abril, G., Stech, J. L., Alvalá, P. C. and Ometto, J. P.: The effects of river inflow and retention time on the spatial heterogeneity of chlorophyll and water–air CO₂ fluxes in a tropical hydropower reservoir, *Biogeosciences*, 12(1), 147–162, doi:10.5194/bg-12-147-2015, 2015.
- 695 Paranaíba, J. R., Barros, N., Mendonça, R., Linkhorst, A., Isidorova, A., Roland, F., Almeida, R. M. and Sobek, S.: Spatially Resolved Measurements of CO₂ and CH₄ Concentration and Gas-Exchange Velocity Highly Influence Carbon-Emission Estimates of Reservoirs, *Environ. Sci. Technol.*, 52(2), 607–615, doi:10.1021/acs.est.7b05138, 2018.
- Pasche, N., Hofmann, H., Bouffard, D., Schubert, C. J., Lozovik, P. A. and Sobek, S.: Implications of river intrusion and convective mixing on the spatial and temporal variability of under-ice CO₂, *Inl. Waters*, 2041, doi:10.1080/20442041.2019.1568073, 2019.

- 700 Pebesma, E. J.: Multivariable geostatistics in S: the gstat package, *Comput. Geosci.*, 30(7), 683–691, doi:10.1016/j.cageo.2004.03.012, 2004.
- Prairie, Y. T., Duarte, C. M. and Kalff, J.: Unifying Nutrient–Chlorophyll Relationships in Lakes, *Can. J. Fish. Aquat. Sci.*, 46(7), 1176–1182, doi:10.1139/f89-153, 1989.
- 705 Prairie, Y. T., Bird, D. F. and Cole, J. J.: The summer metabolic balance in the epilimnion of southeastern Quebec lakes, *Limnol. Oceanogr.*, 47(1), 316–321, doi:10.4319/lo.2002.47.1.0316, 2002.
- Prairie, Y. T., Alm, J., Beaulieu, J., Barros, N., Battin, T., Cole, J., del Giorgio, P., DelSontro, T., Guérin, F., Harby, A., Harrison, J., Mercier-Blais, S., Serça, D., Sobek, S. and Vachon, D.: Greenhouse Gas Emissions from Freshwater Reservoirs: What Does the Atmosphere See?, *Ecosystems*, 21(5), 1058–1071, doi:10.1007/s10021-017-0198-9, 2018.
- 710 Pu, J., Li, J., Zhang, T., Martin, J. B. and Yuan, D.: Varying thermal structure controls the dynamics of CO₂ emissions from a subtropical reservoir, south China, *Water Res.*, 115831, doi:10.1016/j.watres.2020.115831, 2020.
- R Core Team: R: A language and environment for statistical computing, [online] Available from: <https://www.r-project.org/>, 2017.
- 715 Rasilo, T., Hutchins, R. H. S., Ruiz-González, C. and del Giorgio, P. A.: Transport and transformation of soil-derived CO₂, CH₄ and DOC sustain CO₂ supersaturation in small boreal streams, *Sci. Total Environ.*, 579, 902–912, doi:10.1016/j.scitotenv.2016.10.187, 2017.
- Raymond, P. A., Hartmann, J., Lauerwald, R., Sobek, S., McDonald, C., Hoover, M., Butman, D., Striegl, R., Mayorga, E., Humborg, C., Kortelainen, P., Dürr, H., Meybeck, M., Ciais, P. and Guth, P.: Global carbon dioxide emissions from inland waters, *Nature*, 503(7476), 355–359, doi:10.1038/nature12760, 2013.
- 720 Reis, P. C. J., Thottathil, S. D., Ruiz-González, C. and Prairie, Y. T.: Niche separation within aerobic methanotrophic bacteria across lakes and its link to methane oxidation rates, *Environ. Microbiol.*, 22(2), 738–751, doi:10.1111/1462-2920.14877, 2020.
- Roland, F., Vidal, L. O., Pacheco, F. S., Barros, N. O., Assireu, A., Ometto, J. P. H. B., Cimbleris, A. C. P. and Cole, J. J.: Variability of carbon dioxide flux from tropical (Cerrado) hydroelectric reservoirs, *Aquat. Sci.*, 72(3), 283–293, doi:10.1007/s00027-010-0140-0, 2010.
- 725 Rudorff, C. M., Melack, J. M., MacIntyre, S., Barbosa, C. C. F. and Novo, E. M. L. M.: Seasonal and spatial variability of CO₂ emission from a large floodplain lake in the lower Amazon, *J. Geophys. Res. Biogeosciences*, 116(4), 1–12, doi:10.1029/2011JG001699, 2011.

Sand-Jensen, K. and Staehr, P. A.: Net heterotrophy in small danish lakes: A widespread feature over gradients in trophic status and land cover, *Ecosystems*, 12(2), 336–348, doi:10.1007/s10021-008-9226-0, 2009.

730 Sarawak Government: The Geography of Sarawak, [online] Available from: https://www.sarawak.gov.my/web/home/article_view/159/176/ (Accessed 3 May 2019), 2019.

Schmid, M., De Batist, M., Granin, N. G., Kapitanov, V. A., McGinnis, D. F., Mizandrontsev, I. B., Obzhairov, A. I. and Wüest, A.: Sources and sinks of methane in Lake Baikal: A synthesis of measurements and modeling, *Limnol. Oceanogr.*, 52(5), 1824–1837, doi:10.4319/lo.2007.52.5.1824, 2007.

735 Solomon, C. T., Bruesewitz, D. A., Richardson, D. C., Rose, K. C., Van de Bogert, M. C., Hanson, P. C., Kratz, T. K., Larget, B., Adrian, R., Leroux Babin, B., Chiu, C. Y., Hamilton, D. P., Gaiser, E. E., Hendricks, S., Istvá, V., Laas, A., O'Donnell, D. M., Pace, M. L., Ryder, E., Staehr, P. A., Torgersen, T., Vanni, M. J., Weathers, K. C. and Zhu, G.: Ecosystem respiration: Drivers of daily variability and background respiration in lakes around the globe, *Limnol. Oceanogr.*, 58(3), 849–866, doi:10.4319/lo.2013.58.3.0849, 2013.

740 Soued, C. and Prairie, Y. T.: The carbon footprint of a Malaysian tropical reservoir: measured versus modelled estimates highlight the underestimated key role of downstream processes, *Biogeosciences*, 17(2), 515–527, doi:10.5194/bg-17-515-2020, 2020.

Staehr, P. A. and Sand-Jensen, K.: Temporal dynamics and regulation of lake metabolism, *Limnol. Oceanogr.*, 52(1), 108–120, doi:10.4319/lo.2007.52.1.0108, 2007.

745 Tan, A. C.: Water and sediment quality of Batang Ai Reservoir. [online] Available from: <https://ir.unimas.my/id/eprint/10428/>, 2015.

Tang, K. W., McGinnis, D. F., Frindte, K., Brüchert, V. and Grossart, H. P.: Paradox reconsidered: Methane oversaturation in well-oxygenated lake waters, *Limnol. Oceanogr.*, 59(1), 275–284, doi:10.4319/lo.2014.59.1.0275, 2014.

Tank, J. L., Rosi-Marshall, E. J., Griffiths, N. A., Entrekin, S. A. and Stephen, M. L.: A review of allochthonous organic matter dynamics and metabolism in streams, *J. North Am. Benthol. Soc.*, 29(1), 118–146, doi:10.1899/08-170.1, 2010.

750 Teodoru, C. R., Prairie, Y. T. and del Giorgio, P. A.: Spatial Heterogeneity of Surface CO₂ Fluxes in a Newly Created Eastmain-1 Reservoir in Northern Quebec, Canada, *Ecosystems*, 14(1), 28–46, doi:10.1007/s10021-010-9393-7, 2011.

Thornton, K. W., Kimmel, B. L. and Payne, F. E.: *Reservoir Limnology: Ecological Perspectives*, John Wiley & Sons, Inc., 1990.

- 755 Thottathil, S. D., Reis, P. C. J., del Giorgio, P. A. and Prairie, Y. T.: The Extent and Regulation of Summer Methane Oxidation in Northern Lakes, *J. Geophys. Res. Biogeosciences*, 123(10), 3216–3230, doi:10.1029/2018JG004464, 2018.
- Thottathil, S. D., Reis, P. C. J. and Prairie, Y. T.: Methane oxidation kinetics in northern freshwater lakes, *Biogeochemistry*, 143(1), 105–116, doi:10.1007/s10533-019-00552-x, 2019.
- Tranvik, L. J., Cole, J. J. and Prairie, Y. T.: The study of carbon in inland waters-from isolated ecosystems to players in the global carbon cycle, *Limnol. Oceanogr. Lett.*, 3(3), 41–48, doi:10.1002/lol2.10068, 2018.
- 760 Vachon, D. and del Giorgio, P. A.: Whole-Lake CO₂ Dynamics in Response to Storm Events in Two Morphologically Different Lakes, *Ecosystems*, 17(8), 1338–1353, doi:10.1007/s10021-014-9799-8, 2014.
- Vachon, D., Langenegger, T., Donis, D. and McGinnis, D. F.: Influence of water column stratification and mixing patterns on the fate of methane produced in deep sediments of a small eutrophic lake, *Limnol. Oceanogr.*, 64(5), 2114–2128, doi:10.1002/lno.11172, 2019.
- 765 Vachon, D., Sadro, S., Bogard, M. J., Lapierre, J., Baulch, H. M., Rusak, J. A., Denfeld, B. A., Laas, A., Klaus, M., Karlsson, J., Weyhenmeyer, G. A. and Giorgio, P. A.: Paired O₂–CO₂ measurements provide emergent insights into aquatic ecosystem function, *Limnol. Oceanogr. Lett.*, doi:10.1002/lol2.10135, 2020.
- Venkiteswaran, J. J., Schiff, S. L., St. Louis, V. L., Matthews, C. J. D., Boudreau, N. M., Joyce, E. M., Beaty, K. G. and Bodaly, R. A.: Processes affecting greenhouse gas production in experimental boreal reservoirs, *Global Biogeochem. Cycles*, 27(2), 567–577, doi:10.1002/gbc.20046, 2013.
- 770 Wang, Q., Dore, J. E. and McDermott, T. R.: Methylphosphonate metabolism by *Pseudomonas* sp. populations contributes to the methane oversaturation paradox in an oxic freshwater lake, *Environ. Microbiol.*, 19(6), 2366–2378, doi:10.1111/1462-2920.13747, 2017.
- Wilkinson, G. M., Buelo, C. D., Cole, J. J. and Pace, M. L.: Exogenously produced CO₂ doubles the CO₂ efflux from three north temperate lakes, *Geophys. Res. Lett.*, 43(5), 1996–2003, doi:10.1002/2016GL067732, 2016.
- Williams, P. J. I. and Robertson, J. E.: Overall planktonic oxygen and carbon dioxide metabolisms: the problem of reconciling observations and calculations of photosynthetic quotients, *J. Plankton Res.*, doi:10.1093/oxfordjournals.plankt.a042366, 1991.
- Winslow, L., Read, J., Woolway, R., Brenttrup, J., Leach, T., Zwart, J., Albers, S. and Collinge, D.: rLakeAnalyzer: Lake Physics Tools, [online] Available from: <https://cran.r-project.org/package=rLakeAnalyzer>, 2018.
- 780 Wüest, A. and Lorke, A.: Small-Scale Turbulence and Mixing: Energy Fluxes in Stratified Lakes, in *Encyclopedia of Inland*

Waters, pp. 628–635, Elsevier., 2009.

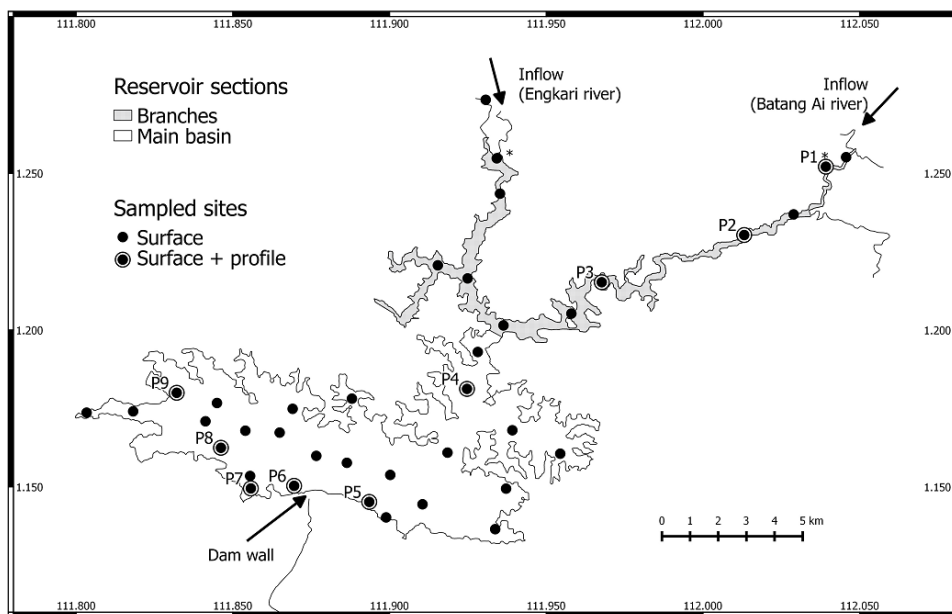
Yao, M., Henny, C. and Maresca, J. A.: Freshwater Bacteria Release Methane as a By-Product of Phosphorus Acquisition, edited by J. E. Kostka, *Appl. Environ. Microbiol.*, 82(23), 6994–7003, doi:10.1128/AEM.02399-16, 2016.

785 Zarfl, C., Lumsdon, A. E., Berlekamp, J., Tydecks, L. and Tockner, K.: A global boom in hydropower dam construction, *Aquat. Sci.*, 77(1), 161–170, doi:10.1007/s00027-014-0377-0, 2015.

Zhang, Q., Tao, Z., Ma, Z., Gao, Q., Deng, H., Xu, P., Ding, J., Wang, Z. and Lin, Y.: Hydro-ecological controls on riverine organic carbon dynamics in the tropical monsoon region, *Sci. Rep.*, 9(1), 1–11, doi:10.1038/s41598-019-48208-y, 2019.

790 **Table 1: Mean (\pm SD) of physical and chemical variables measured at the surface of the three reservoir sections.**

Variables	Units	Inflows	Branches	Main basin
Zepi	m	1.3 (\pm 1.6)	8 (\pm 2.3)	10.6 (\pm 1.7)
Secchi	m	1.2 (\pm 0.9)	5.1 (\pm 1.2)	5.5 (\pm 1.2)
Temperature	$^{\circ}$ C	27.1 (\pm 2.5)	30.7 (\pm 0.5)	30.6 (\pm 0.5)
pH		6.5 (\pm 0.3)	7.2 (\pm 0.2)	7.2 (\pm 0.2)
O ₂	%	94.9 (\pm 7.7)	102.7 (\pm 4.5)	99.3 (\pm 4.8)
DOC	mg L ⁻¹	0.8 (\pm 0.4)	0.9 (\pm 0.2)	0.9 (\pm 0.2)
TP	μ g L ⁻¹	20.7 (\pm 7.6)	6.2 (\pm 1.7)	5.8 (\pm 2.6)
TN	mg L ⁻¹	0.14 (\pm 0.04)	0.12 (\pm 0.04)	0.1 (\pm 0.03)
Chla	μ g L ⁻¹	2.1 (\pm 1.7)	1.7 (\pm 1)	1.2 (\pm 0.5)



795 **Figure 1: Map of Batang Ai reservoir with delimited sections (branches and main basin) and sampling points. * Represents sampling points at the branches extremities.**

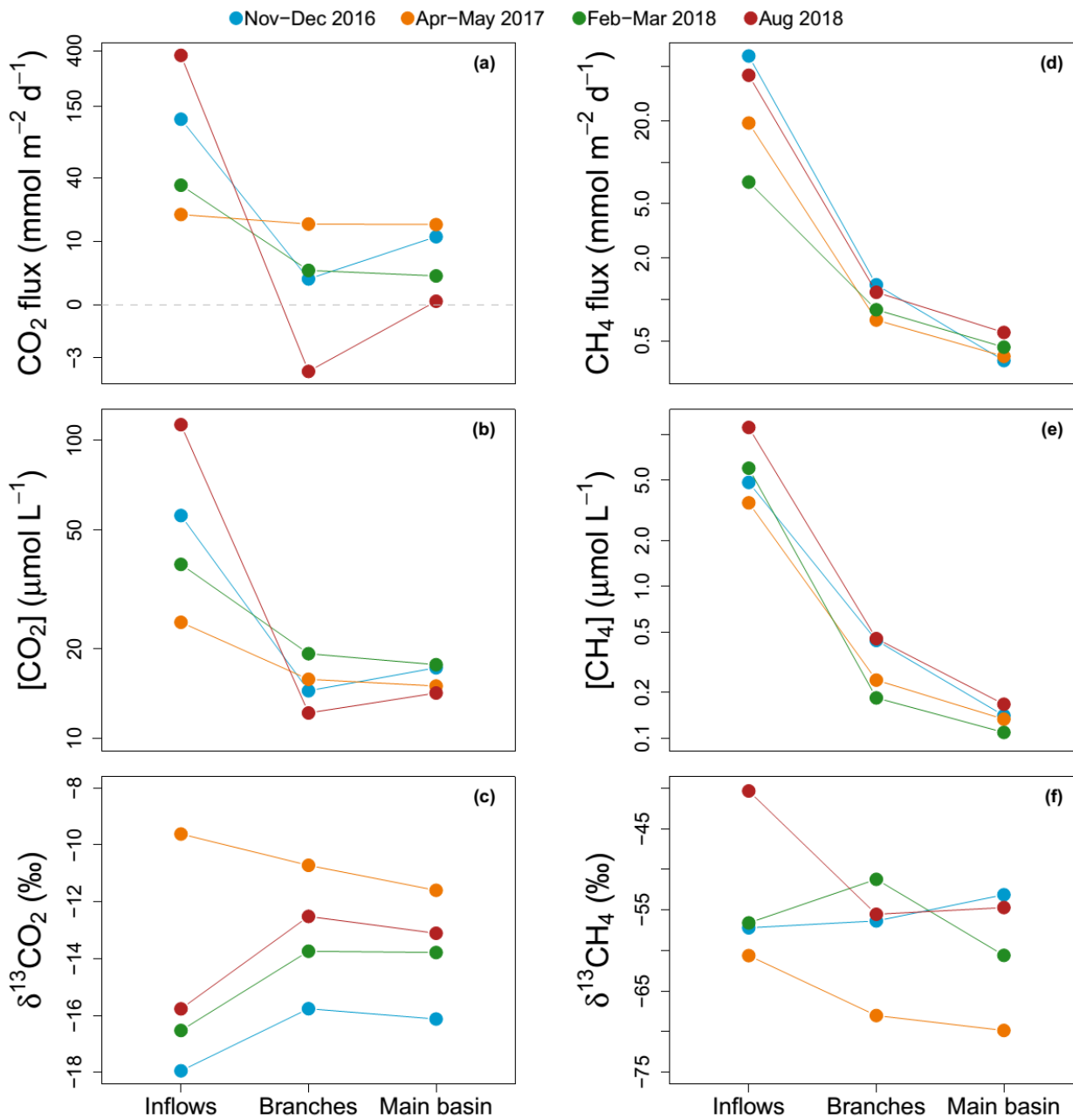
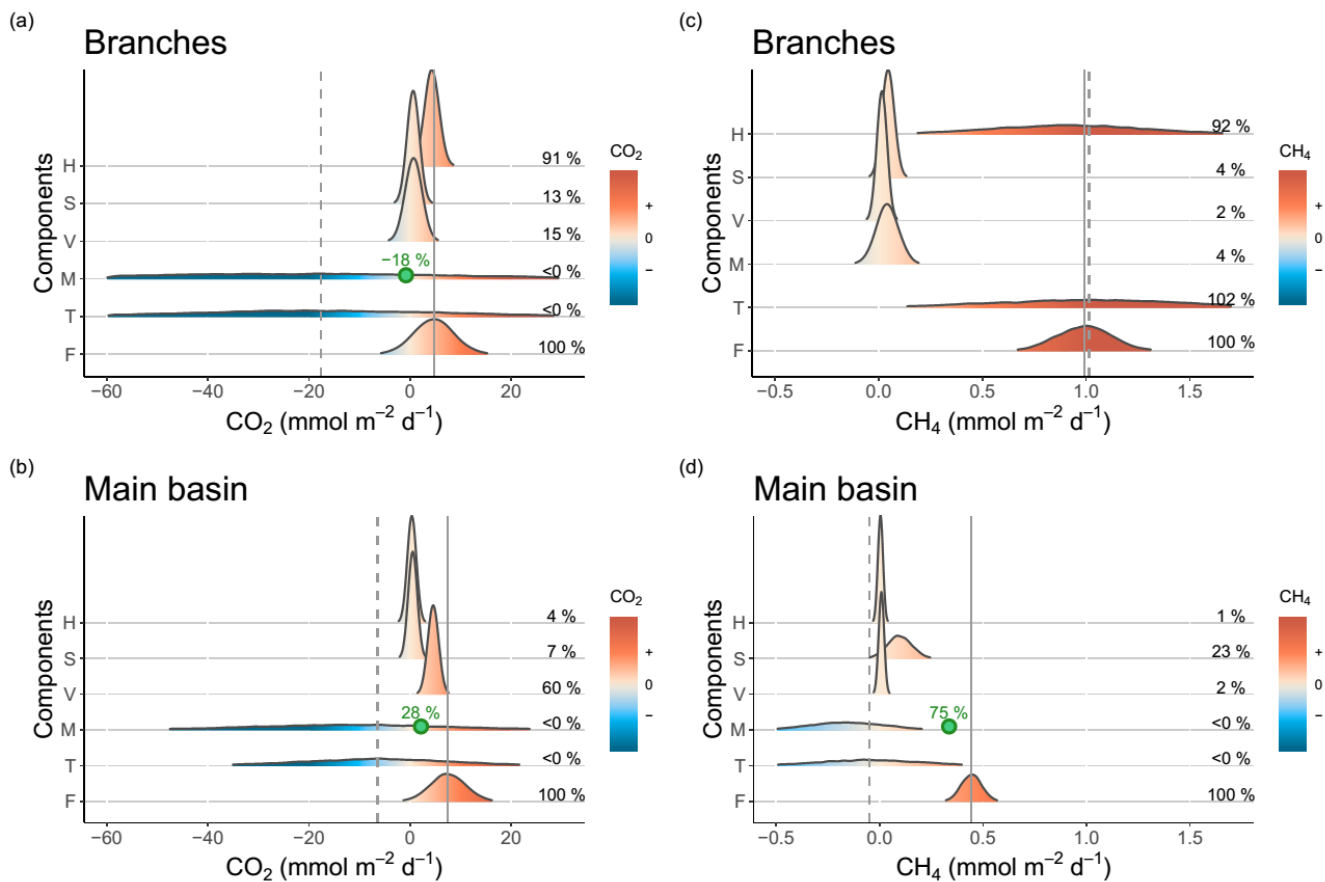
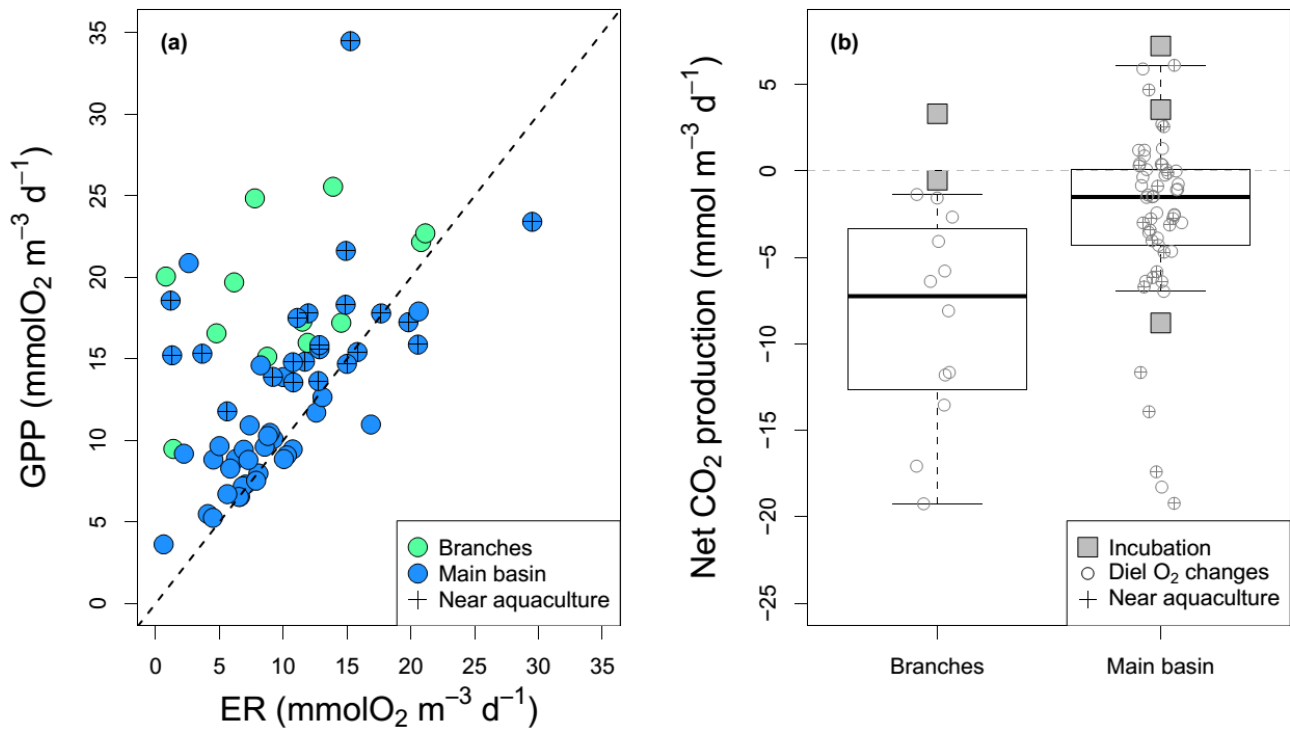


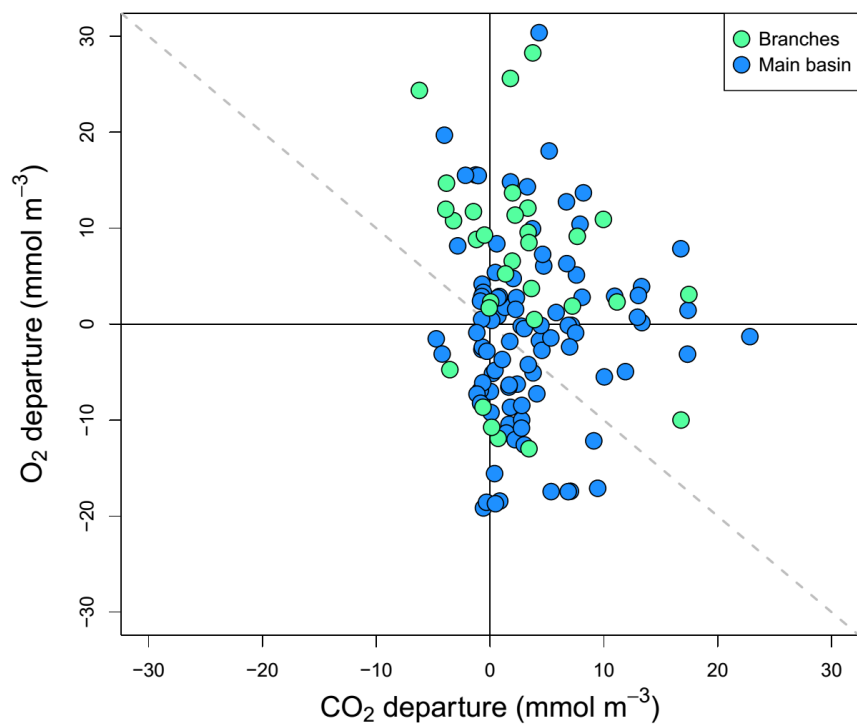
Figure 2: Average of spatially interpolated surface CO₂ (a, b, c) and CH₄ (d, e, f) fluxes (a, d), concentrations (b, e), and isotopic signatures (c, f) along the hydrological continuum from the reservoir inflows to the main basin for each sampling campaign.



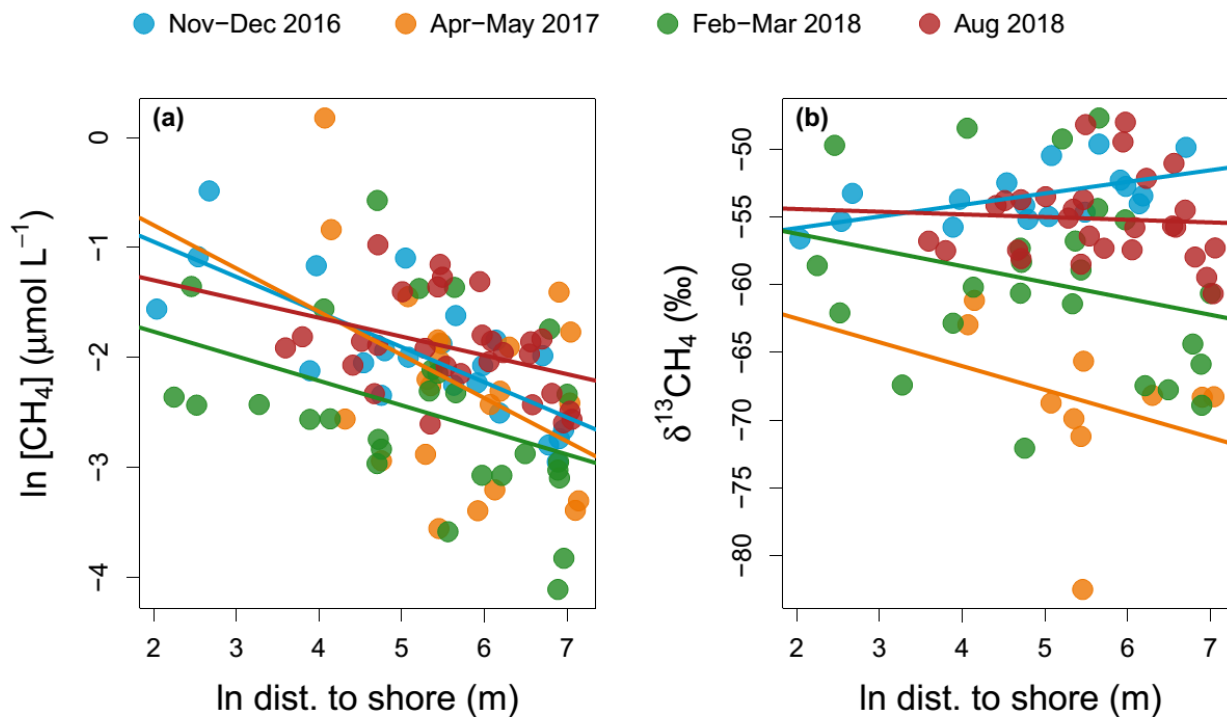
805 **Figure 3: Density distributions of the different components of CO₂ (a, b) and CH₄ (c, d) surface budgets in the reservoir branches**
 (a, c) and main basin (b, d). Components are: H = horizontal flow inputs, S = sediment inputs, V = vertical inputs, M = net metabolism
 (average of the incubation and diel O₂ monitoring methods), T = sum of all estimated sources and processes in the surface layer, and
 F = measured surface fluxes. Density curves are based on simulated normal distributions using the mean and standard error of each
 810 component. The x-axes represent the areal rate of CO₂ or CH₄ and the color scale indicates the sign of the rate. Mean values of the
 fraction of each component (in %) relative to the mean surface flux (F) are reported on the right side in each panel. The solid and
 dashed grey lines represent the means of F and T respectively. In panels a, b, and d, the point and % in green represent the
 hypothetical value of the M rate (the most uncertain component) and its corresponding fraction (as % of F) that are needed to close
 the budget (to obtain T = F).



815 **Figure 4: Epilimnetic daily GPP versus ER rates (a) derived from diel O_2 changes in the reservoir branches and main basin (including sites near aquacultures), with the 1:1 line (dotted). Panel (b) shows boxplots of the corresponding rates of CO_2 NEP in the branches and main basin, with boxes bounds, whiskers, solid line, and open circles, and squares representing the 25th and 75th percentiles, the 10th and 90th percentiles, the median, single data points (diel O_2 method), and incubation derived rates respectively.**



820 **Figure 5: Surface O₂ versus CO₂ departure from saturation for all sampled surface sites in the reservoir main basin and branches across all sampling campaigns.**



825 **Figure 6: Regression of CH₄ concentration (a) and isotopic signature (b) as a function of distance to shore in each sampling campaign in the main reservoir basin. For CH₄ concentration, regressions lines have the following statistics in order of sampling: p-values: < 0.001, 0.06, 0.03, 0.05, and R²_{adj}: 0.54, 0.13, 0.11. For δ¹³CH₄, all regressions had p-values > 0.2 except for the Nov-Dec 2016 campaign with p-value = 0.01 and R²_{adj} = 0.29.**